RSC Advances

PAPER

View Article Online
View Journal | View Issue

Cite this: *RSC Adv.*, 2024, **14**, 30346

Design, synthesis, biological evaluation, and docking studies of novel triazolo[4,3-*b*]pyridazine derivatives as dual c-Met/Pim-1 potential inhibitors with antitumor activity†

Mohamed E. Mahmoud,[a] Eman M. Ahmed,[b] Hamdy M. Ragab,[b] Rania Farag A. Eltelbany[c] and Rasha A. Hassan *[b]

Received 1st June 2024
Accepted 17th September 2024

DOI: 10.1039/d4ra04036h

rsc.li/rsc-advances

Interest has been piqued in c-Met and Pim-1, potential new cancer treatment targets. A variety of triazolo[4,3-*b*]pyridazine derivatives were synthesized to create powerful dual c-Met/Pim-1 inhibitors having the pharmacophoric elements of both enzyme inhibitors. All derivatives were screened for their cytotoxic effects on 60 cancer cell lines. Compounds **4g** and **4a**, had strong antiproliferative cytotoxic impacts on tumor cells, with mean GI% values of 55.84 and 29.08%, respectively. Research revealed that **4g** has more powerful inhibitory activity against c-Met and Pim-1, with IC_{50} of 0.163 ± 0.01 and 0.283 ± 0.01 μM, respectively than the reference and derivative **4a**. Moreover, compound **4g** was the subject of an additional investigation into biological processes. The findings showed that compound **4g** caused MCF-7 cells to arrest in the S stage of the cell cycle. Also, it accelerated the progress of apoptosis 29.61-fold more than the control. Compound **4g** demonstrated a significantly higher level of caspase-9 and a decreased level of *p*-PI3K, *p*-AKT, and *p*-mTOR compared to staurosporine. Later, analysis of **4g** showed good drug-ability and pharmacokinetic properties. A similar mode of interaction at the ATP-binding site of c-Met and Pim-1 compared to the docked ligands was suggested by additional docking studies of compound **4g**.

1. Introduction

Breast cancer is the most prevalent cancer in women diagnosed globally.[1] Most of them can be identified early enough to be successfully treated; nevertheless, many patients may not benefit from the medication, and metastasis ultimately contributes to death.[2] The life expectancy of patients with breast cancer has not been substantially raised by the now-available therapeutics, which include surgery, radiotherapy, and chemotherapy, and they frequently have detrimental side effects. Most pharmaceutical cancer therapies are cytotoxic. Additionally, multiple complications, such as neuropathy, axillary vein thrombosis, and cardiovascular disease, may develop after radiation or surgical treatments for breast cancer.[3]

Hepatocyte growth factor (HGF) binding stimulates the tyrosine kinase receptor c-Met kinase, which leads to receptor dimerization and subsequent signaling.[4] This pathway is crucial for healthy adult wound healing and normal embryonic development in normal cells.[5] Based on reports, the overexpression of the c-Met kinase receptor deregulates the c-Met kinase pathway in several human cancers. Poor prognosis, tumor proliferation, angiogenesis, and metastasis are all attributed to this deregulation.[6] The analogous proto-oncogenic serine/threonine protein kinases known as Pim kinases 1, 2, and 3 are positive controllers of cell cycle progression and constitutively active enzymes.[7] As oncogenic survival factors, they can inhibit apoptosis. They are crucial in controlling cell proliferation, differentiation, migration, and survival.[8] Pim kinases are abnormally overexpressed in a wide range of solid (including prostate and breast tumors) and hematologic (including multiple myeloma) tumors.[9] Ultimately, this leads to cancer progression, metastasis, drug resistance, and, frequently, a poor prognosis. Notably, drug efflux transporter expression, activation, and stabilization have all been linked to Pim kinases, which contribute to multidrug resistance. Moreover, Pim-1 phosphorylates the breast cancer-resistant protein, which promotes its multimerization and stable membrane expression.[10] Furthermore, due to the duplicated functions of the three Pim isoforms, plenty of interest is shown in developing pan-Pim inhibitors.[11]

[a]*Department of Pharmaceutical Organic Chemistry, Faculty of Pharmacy, Modern University for Technology and Information (MTI), Cairo, Egypt*

[b]*Department of Pharmaceutical Organic Chemistry, Faculty of Pharmacy, Cairo University, Cairo, Egypt. E-mail: rasha.hasan@pharma.cu.edu.eg*

[c]*Department of Biochemistry, Faculty of Pharmacy, Modern University for Technology and Information (MTI), Cairo, Egypt*

† Electronic supplementary information (ESI) available. See DOI: https://doi.org/10.1039/d4ra04036h

Cellular signaling pathways are closely correlated with one another to enable multicellular functions like cell division, cell fate determination, and cell migration. Pathologies, including cancer, may result from erroneous signal transfer within the cell, and this dysregulation results in the incorrect signaling of many other protein degradation pathways, such as PI3K/AKT/mTOR (phosphoinositide 3-kinase/AKT/mechanistic target of rapamycin) signaling.[12]

One of the most frequent genomic mutations in breast cancer across different subtypes is imperfections in the PI3K/AKT/mTOR pathway, which ultimately fosters tumor-cell growth.[13] The PI3K/AKT/mTOR signaling pathway, which is frequently dysregulated in cancer, is essential for regulating cell metabolism, proliferation, and survival.[13,14] PI3Ks are available in 4 isoforms (α, β, δ, and γ) and are heterodimers made up of regulatory (p85) and catalytic (p110) subunits.[13] The agonist effect of receptor tyrosine kinases initiates PI3K activation, which in turn causes phosphorylation of AKT and mTOR complex 1 (mTORC1) to trigger the process. mTOR is an abnormal serine/threonine protein kinase made up of mTOR complex 1 (mTORC1) and mTOR complex 2 (mTORC2).[15]

Although several genes participate in apoptosis, caspases are the principal mediators of the process. The carboxyl side of the aspartate residue is where caspases, aspartate-specific cysteine proteases, fragment their substrates. At present, it is known that there are at least 14 different types of caspases, of which 2/3 are involved in apoptosis. The two primary groups of caspases involved in apoptosis are the upstream initiator caspases (such as caspases 2, 3, and 6) and the downstream effector caspases (such as caspases 8, 9, and 10). The representatives of the latter class are responsible for the morphological changes that occur during apoptosis and destroy numerous cellular proteins.[3]

1,2,4-Triazolo[4,3-*b*]pyridazine derivatives exhibit substantial therapeutic properties like anxiolytic,[16,17] anticonvulsant,[18] antimicrobial,[19,20] and antiviral properties.[21,22] Additionally, they are used as various enzyme inhibitors, such as leucine-rich repeat kinase 2 (LRRK2),[23,24] phosphodiesterase (PDE4),[25] and TRAF6 E3 ligase in autoimmune diseases.[26] During the past twenty years, more attention has focused on the use of triazolopyridazine to design ligands that could be potential anticancer drugs by targeting enzymatic pathways involved in the different pathogenesis stages adopted in the progression of cancer, including metastasis, angiogenesis, and others. The c-Met and Pim-1 enzymes are the most promising novel targeted enzymes for designing new antitumor compounds. The therapeutic potential for c-Met and Pim-1 inhibitors is significant due to their critical roles in cancer progression and therapy resistance. Dual inhibition of c-Met and Pim-1 produces a synergistic effect, where a dual inhibitor can target multiple pathways simultaneously. This can result in greater therapeutic efficacy than targeting either kinase alone. Also, a dual c-Met/Pim-1 inhibitor can minimize the chances of resistance development and offer a promising strategy to enhance anticancer efficacy.[27]

A promising c-Met and Pim-1 inhibitory activity was reported for the previously synthesized compounds **I–III** (ref. 28) and **IV–VI** (ref. 29) (Fig. 1).

Following the above data, it was interesting to continue our research to create potent new anticancer drugs with high therapeutic equivalence.[30–37] The main goal of the current study was to generate new 1,2,4-triazolo[4,3-*b*]pyridazine derivatives that are dual inhibitors of the c-Met and Pim-1 kinases with anticancer activity. The NCI (USA) 60-panel cell line was used as a model to assess the anticancer activities of the developed derivatives, and *in vitro* inhibitory studies using c-Met and Pim-1 enzymes were conducted on the most promising derivatives. We investigated the total concentration and phosphorylated concentration of the PI3K-Akt-mTOR pathway, assessed through the derivatives produced, to delve deeper into the mechanistic pathways of antiproliferative activity. In addition, the effects of these substances, including their impact on the typical cell cycle profile, caspase-9 activity, and apoptosis induction, have been studied in the breast cancer cell line MCF7. In a concluding study, molecular docking confirmed these molecules' binding modes and action targets.

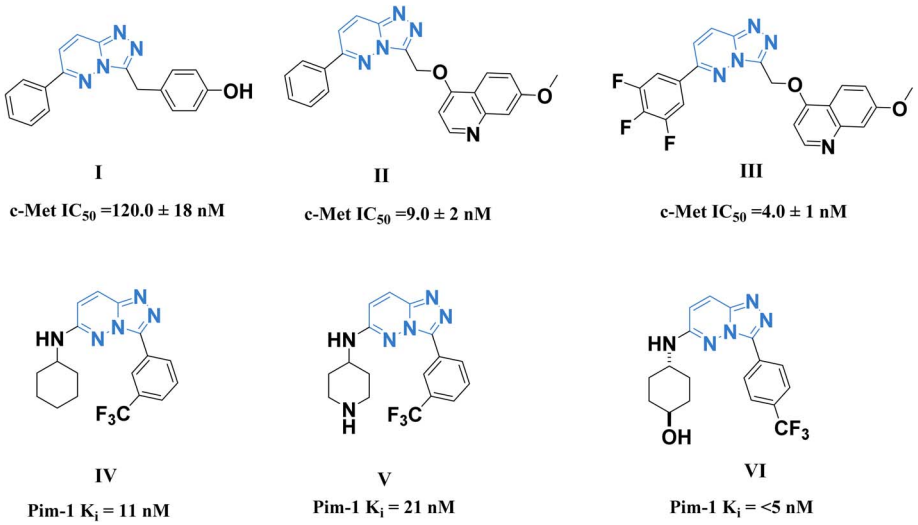

Fig. 1 Some reported 1,2,4-triazolo[4,3-*b*]pyridazine derivatives as c-Met (I–III) and Pim-1 (IV–VI) inhibitors.

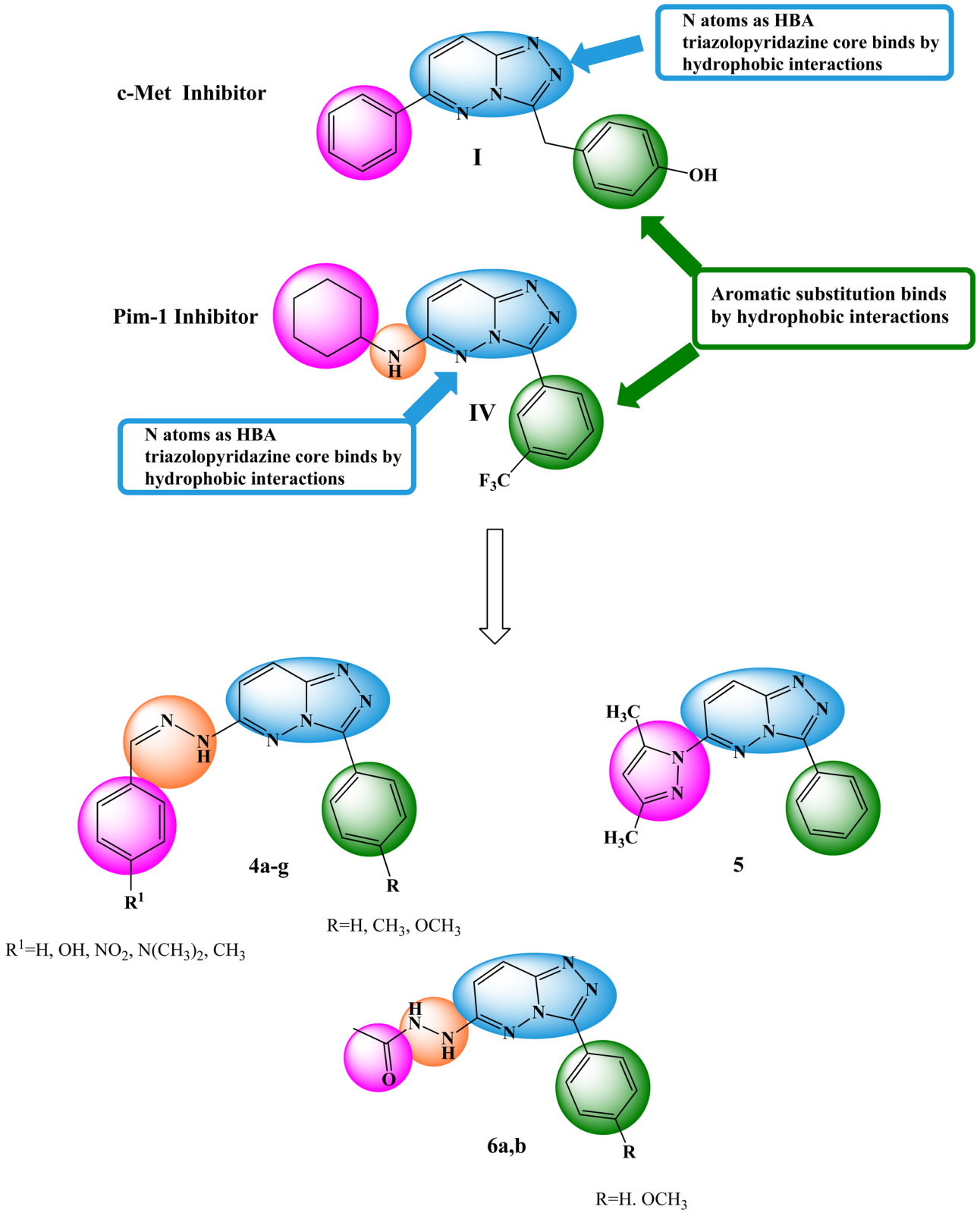

Fig. 2 Basic structural elements of compounds I and IV and modifications to the newly synthesized derivatives.

The primary objective of the molecular design was to customize the lead compounds **I** and **IV** to generate new anti-proliferative drugs that target c-Met and Pim-1 and have greater dual inhibitory activity. The triazolopyridazine core, which formed crucial interactions with important amino acids in the c-Met and Pim-1 active pockets, was preserved as part of the modification strategy (Fig. 2). The replacement of the 3-hydroxybenzyl group in compound **I** and the 3-

trifluoromethylphenyl group in compound **IV** was accomplished using a phenyl group (**4a–c**, **5**, and **6a**) or divergent *para*-substituted phenyl groups, ranging from hydrophilic groups like OCH_3 (**4e–g** and **6b**) to hydrophobic substituents like CH_3 in compound **4d**. On the other hand, the phenyl ring at C6 in compound **I** and the cyclohexyl ring in compound **IV** were replaced by different *para*-substituted phenyl groups in derivatives **4**, the dimethyl pyrazole group in derivative **5**, or the acetyl group in derivatives **6**. Finally, the amino linker in compound **IV** was replaced by an amino azomethine group in derivatives **4**, a hydrazine group in compounds **6a,b**, or removed as in compound **5**. Such replacements were adopted so that the triazolopyridazine core was retained in the proper position inside the active pockets of the two enzymes. The enzymatic interactions were enhanced by the different groups located in position 6, either the donating groups (OH and $N(CH_3)_2$) or the withdrawing groups (NO_2). Finally, hydrogen bond donors and acceptors were incorporated through the OH and NH in various positions or the carbonyl group in acetohydrazide derivatives **6a,b**.

2. Experimental

2.1 Chemistry

2.1.1 General. Starting materials and solvents were acquired from commercial suppliers and were used without extra purification. Melting points were obtained on a Griffin apparatus and were uncorrected. Microanalyses for C, H, and N were carried out at the Regional Center for Mycology and Biotechnology, Faculty of Pharmacy, Al-Azhar University. IR spectra were recorded on Shimadzu IR 435 spectrophotometer, Faculty of Pharmacy, Cairo University, Cairo, Egypt, and values were represented in cm^{-1}. ^1H NMR spectra were carried out on Bruker 400 MHz (Bruker Corp., Billerica, MA, USA) spectrophotometer, Faculty of Pharmacy, Cairo University, Cairo, Egypt. The chemical shifts were recorded in ppm on δ scale, coupling constants (J) were given in Hz, and peak multiplicities are designed as follows: s, singlet; d, doublet; dd, doublet of doublet; t, triplet; m, multiplet. ^{13}C NMR spectra were carried out on Bruker 100 MHz spectrophotometer, Faculty of Pharmacy, Cairo University, Cairo, Egypt. Progress of the reactions was monitored by TLC using precoated aluminum sheet silica gel MERCK 60F 254 and was visualized by UV lamp. The original IR and NMR spectra of the investigated compounds are provided in the ESI.† 6-Chloro-3-hydrazinopyridazine, 3-(2-(4-arylidene)hydrazinyl)-6-chloropyridazine **1a–c**, 6-chloro-3-aryl-[1,2,4]-triazolo[4,3-*b*]pyridazine **2a–c** and 6-hydrazino-3-aryl-[1,2,4]-triazolo[4,3-*b*]pyridazine **3a–c** were prepared as reported in literature.[38–40]

*2.1.1.1 General procedure for the preparation of 6-arylidenehydrazino-3-aryl-[1,2,4]triazolo[4,3-b]pyridazine (**4a–g**).* 6-Hydrazineyl-3-(4-aryl)-[1,2,4]triazolo[4,3-*b*]pyridazine derivatives **3a–c** (0.68 g (**3a**), 0.72 g (**3b**), or 0.76 g (**3c**), 0.003 mol) was heated in 15 mL of absolute ethanol for 10 min. Following complete dissolution, the appropriate aromatic aldehyde such as benzaldehyde, 4-hydroxybenzaldehyde, 4-nitrobenzaldehyde, 4-methylbenzaldehyde or *N*,*N*-dimethylbenzaldehyde (0.003 mol) was added and the reaction mixture was refluxed at 80 °C for 4 h. The reaction was cooled, the crude product was collected through filtration and purified *via* recrystallization from hot ethanol.

*2.1.1.2 3-((2-(3-Phenyl-[1,2,4]triazolo[4,3-b]pyridazin-6-yl) hydrazono)methyl)phenol (**4a**).* Dark yellow solid: 72% yield; m.p. 229–230 °C; IR (KBr, cm^{-1}) 3425 (OH), 3298 (NH), 3051 (CH aromatic), 1631 (C=N), 1604 (C=C); ^1H NMR (400 MHz, DMSO-d_6) δ 11.65 (s, 1H, NH, D_2O exchangeable), 9.97 (s, 1H, OH, D_2O exchangeable), 8.47 (s, 2H, Ar–H), 8.09 (s, 2H, Ar–H), 7.56–7.49 (m, 6H, Ar–H), 6.86 (s, 2H, Ar–H); ^{13}C NMR (100 MHz, DMSO-d_6) δ 159.4, 153.8, 143.6, 130.6, 130.2, 129.1 (2C), 128.7 (2C), 127.8, 127.5 (2C), 126.0, 125.3, 116.2 (2C), 114.2, 109.8. Anal. calcd for $C_{18}H_{14}N_6O$ (330.35): C, 65.44; H, 4.27; N, 25.44; found, C, 65.31; H, 4.52; N, 25.70%.

*2.1.1.3 6-(2-(4-Nitrobenzylidene)hydrazinyl)-3-phenyl-[1,2,4] triazolo[4,3-b]pyridazine (**4b**).* Canary yellow solid: 70%; m.p. 226–227 °C; IR (KBr, cm^{-1}) 3390 (NH), 3051 (CH aromatic), 1631 (C=N), 1554 (C=C), 1530, 1338 (NO_2); ^1H NMR (400 MHz, DMSO-d_6) δ 12.15 (s, 1H, NH, D_2O exchangeable), 8.45 (d, J = 7.6 Hz, 2H, Ar–H), 8.31 (d, J = 8.0 Hz, 1H, Ar–H), 8.24 (s, 1H, CH = N), 8.22 (d, J = 6.4 Hz, 2H, Ar–H), 7.95 (d, J = 8.0 Hz, 2H, Ar–H), 7.67 (d, J = 8.0 Hz, 1H, Ar–H), 7.63–7.59 (m, 2H, Ar–H), 7.56 (d, J = 7.6 Hz, 1H, Ar–H); ^{13}C NMR (100 MHz, DMSO-d_6) δ 160.7, 153.8, 147.6, 146.4, 141.4, 130.3, 130.0, 129.1 (2C), 127.6 (2C), 127.4 (2C), 126.9, 126.0, 124.4 (2C), 113.9. Anal. calcd for $C_{18}H_{13}N_7O_2$ (359.35): C, 60.16; H, 3.65; N, 27.29; found, C, 60.37; H, 3.84; N, 27.11%.

*2.1.1.4 N,N-Dimethyl-4-((2-(3-phenyl-[1,2,4]triazolo[4,3-b] pyridazin-6-yl)hydrazono)methyl)aniline (**4c**).* Reddish brown solid: 72%; m.p. 271–272 °C; IR (KBr, cm^{-1}) 3425 (NH), 3061 (CH aromatic), 2966, 2893 (CH aliphatic), 1612 (C=N), 1566 (C=C); ^1H NMR (400 MHz, DMSO-d_6) δ 11.36 (s, 1H, NH, D_2O exchangeable), 8.50 (d, J = 6.8 Hz, 2H, Ar–H), 8.20 (d, J = 9.2 Hz, 1H, Ar–H), 8.05 (s, 1H, CH = N), 7.61–7.55 (m, 6H, Ar–H), 6.76 (d, J = 8.0 Hz, 2H, Ar–H), 2.98 (s, 6H, $N(CH_3)_2$); ^{13}C NMR (100 MHz, DMSO-d_6) δ 151.6, 146.4, 144.1, 130.1, 129.1 (2C), 128.3 (2C), 127.3 (2C), 125.6, 122.5, 121.6, 114.1, 113.0, 112.4 (2C), 106.1, 40.4 (2C). Anal. calcd for $C_{20}H_{19}N_7$ (357.42): C, 67.21; H, 5.36; N, 27.43; found, C, 67.43; H, 5.50; N, 27.69%.

*2.1.1.5 6-(2-Benzylidenehydrazinyl)-3-(p-tolyl)-[1,2,4]triazolo [4,3-b]pyridazine (**4d**).* Yellow solid: 74% yield; m.p. 269–270 °C; IR (KBr, cm^{-1}) 3429 (NH), 3151, 3028 (CH aromatic), 2920, 2893 (CH aliphatic), 1631 (C=N), 1562 (C=C); ^1H NMR (400 MHz, DMSO-d_6) δ 11.68 (s, 1H, NH, D_2O exchangeable), 8.39 (d, J = 6.8 Hz, 2H, Ar–H), 8.25 (d, J = 9.5 Hz, 1H, Ar–H), 8.17 (s, 1H, CH = N), 7.76 (d, J = 6.4 Hz, 2H, Ar–H), 7.60 (d, J = 8.0 Hz, 1H, Ar–H), 7.47–7.41 (m, 5H, Ar–H), 2.42 (s, 3H, CH_3); ^{13}C NMR (100 MHz, DMSO-d_6) δ 153.9, 146.5, 144.5, 142.9, 139.8, 135.1, 129.8, 129.7 (2C), 129.3 (2C), 127.2 (2C), 127.0 (2C), 126.0, 124.5, 113.6, 21.5. Anal. calcd for $C_{19}H_{16}N_6$ (328.38): C, 69.50; H, 4.91; N, 25.59; found, C, 69.67; H, 5.05; N, 25.78%.

*2.1.1.6 6-(2-Benzylidenehydrazinyl)-3-(4-methoxyphenyl)-[1,2,4]triazolo[4,3-b]pyridazine (**4e**).* Off-white solid: 75% yield; m.p. 267–268 °C; IR (KBr, cm^{-1}) 3425 (NH), 3151, 3039 (CH aromatic), 2997, 2920 (CH aliphatic), 1631 (C=N), 1556 (C=C); ^1H NMR (400 MHz, DMSO-d_6) δ 11.67 (s, 1H, NH, D_2O

exchangeable), 8.42 (d, J = 8.4 Hz, 2H, Ar–H), 8.22 (d, J = 9.8 Hz, 1H, Ar–H), 8.16 (s, 1H, CH = N), 7.75 (d, J = 6.8 Hz, 2H, Ar–H), 7.58 (d, J = 9.8 Hz, 1H, Ar–H), 7.47–7.39 (m, 3H, Ar–H), 7.14 (d, J = 8.8 Hz, 2H, Ar–H), 3.86 (s, 3H, OCH_3); ^{13}C NMR (100 MHz, DMSO-d_6) δ 160.7, 153.9, 146.4, 144.4, 142.8, 135.1, 129.8, 129.3 (2C), 128.9 (2C), 127.0 (2C), 125.9, 119.7, 114.5 (2C), 113.4, 55.8. Anal. calcd for $C_{19}H_{16}N_6O$ (344.38): C, 66.27; H, 4.68; N, 24.40; found, C, 66.09; H, 4.79; N, 24.63%.

*2.1.1.7 3-(4-Methoxyphenyl)-6-(2-(4-methylbenzylidene)hydrazinyl)-[1,2,4]triazolo[4,3-b]pyridazine (**4f**).* Dark brown solid: 72% yield; m.p. 230–231 °C; IR (KBr, cm^{-1}) 3425 (NH), 3151, 3036 (CH aromatic), 2916, 2893 (CH aliphatic), 1616 (C=N), 1562 (C=C); ^{1}H NMR (400 MHz, DMSO-d_6) δ 11.60 (s, 1H, NH, D_2O exchangeable), 8.43 (d, J = 4.8 Hz, 2H, Ar–H), 8.20 (d, J = 6.4 Hz, 1H, Ar–H), 8.13 (s, 1H, CH = N), 7.63–7.53 (m, 3H, Ar–H), 7.26 (d, J = 4.8 Hz, 2H, Ar–H), 7.15 (d, J = 5.6 Hz, 2H, Ar–H), 3.87 (s, 3H, OCH_3), 2.34 (s, 3H, CH_3); ^{13}C NMR (100 MHz, DMSO-d_6) δ 160.7, 153.9, 152.4, 146.5, 142.9, 139.5, 132.4 (2C), 129.9 (2C), 128.9 (2C), 126.9, 125.9, 119.7, 114.5 (2C), 113.5, 55.8, 21.5. Anal. calcd for $C_{20}H_{18}N_6O$ (358.41): C, 67.02; H, 5.06; N, 23.45; found, C, 67.23; H, 5.29; N, 23.73%.

*2.1.1.8 4-((2-(3-(4-Methoxyphenyl)-[1,2,4]triazolo[4,3-b]pyridazin-6-yl)hydrazono)methyl)phenol (**4g**).* Yellow solid: 70% yield; m.p. 224–225 °C; IR (KBr, cm^{-1}) 3491 (OH), 3332 (NH), 3055 (CH aromatic), 2966, 2931 (CH aliphatic), 1631 (C=N), 1562 (C=C); ^{1}H NMR (400 MHz, DMSO-d_6) δ 11.42 (s, 1H, NH, D_2O exchangeable), 9.96 (s, 1H, OH, D_2O exchangeable), 8.42 (d, J = 8.8 Hz, 2H, Ar–H), 8.17 (d, J = 9.6 Hz, 1H, Ar–H), 8.07 (s, 1H, CH = N), 7.58 (d, J = 8.4 Hz, 2H, Ar–H), 7.52 (d, J = 9.6 Hz, 1H, Ar–H), 7.14 (d, J = 8.4 Hz, 2H, Ar–H), 6.85 (d, J = 8.4 Hz, 2H, Ar–H), 3.86 (s, 3H, OCH_3); ^{13}C NMR (100 MHz, DMSO-d_6) δ 160.7, 159.3, 153.9, 146.4, 144.3, 143.5, 129.0 (2C), 128.7 (2C), 126.1, 125.6, 119.6, 116.2 (2C), 114.5 (2C), 113.8, 55.8. Anal. calcd for $C_{19}H_{16}N_6O_2$ (360.38): C, 63.32; H, 4.48; N, 23.32; found, C, 63.57; H, 4.41; N, 23.60%.

*2.1.1.9 Preparation of 6-(3,5-dimethyl-1H-pyrazol-1-yl)-3-phenyl-[1,2,4]triazolo[4,3-b]pyridazine (**5**).* Acetyl acetone (0.7 g, 0.007 mol) was added to a solution of 6-hydrazineyl-3-(4-aryl)-[1,2,4]triazolo[4,3-*b*]pyridazine derivatives **3a–c** (0.007 mol) in absolute ethanol (10 mL), and the reaction mixture was refluxed at 80 °C for 6 h. The mixture was allowed to cool at room temperature, and the product was filtered, dried, and recrystallized from ethanol to give a buff solid: 80% yield; m.p. 139–140 °C; IR (KBr, cm^{-1}) 3047 (CH aromatic), 2962, 2927 (CH aliphatic), 1624 (C=N), 1543 (C=C); ^{1}H NMR (400 MHz, DMSO-d_6) δ 8.48 (d, J = 9.2 Hz, 1H, Ar–H), 8.29 (s, 2H, Ar–H), 7.96 (d, J = 8.8 Hz, 1H, Ar–H), 7.62 (d, J = 3.6 Hz, 3H, Ar–H), 6.26 (s, 1H, CH pyrazole), 2.63 (s, 3H, CH_3), 2.23 (s, 3H, CH_3); ^{13}C NMR (100 MHz, DMSO-d_6) δ 151.5, 150.4, 147.8, 144.3, 142.1, 130.7, 129.2 (2C), 127.8 (2C), 127.1, 126.3, 117.3, 111.3, 14.8, 13.8. Anal. calcd for $C_{16}H_{14}N_6$ (290.33): C, 66.19; H, 4.86; N, 28.95; found, C, 65.98; H, 5.02; N, 29.17%.

*2.1.1.10 General procedure for the preparation of [1,2,4]triazolo[4,3-b]pyridazine acetohydrazide (**6a,b**).* Acetic anhydride (0.714 g, 0.007 mol) was added to a solution of 6-hydrazineyl-3-(4-aryl)-[1,2,4]triazolo[4,3-*b*]pyridazine derivatives **3a–c** (0.007 mol) in glacial acetic acid (10 mL), and the reaction mixture was heated under reflux at 120 °C for 6 h. The mixture was poured into 20 mL of ice-cold water. After filtration, drying, and recrystallization from ethanol, the final crude product was produced.

*2.1.1.11 N′-(3-Phenyl-[1,2,4]triazolo[4,3-b]pyridazin-6-yl) acetohydrazide (**6a**).* Buff solid: 75% yield, m.p. 159–160 °C; IR (KBr, cm^{-1}) 3383, 3232 (2 NH), 3097 (CH aromatic), 2993 (CH aliphatic), 1685 (C=O), 1631 (C=N), 1589 (C=C); ^{1}H NMR (400 MHz, DMSO-d_6) δ 9.72 (s, 1H, NH, D_2O exchangeable), 8.44 (d, J = 7.6 Hz, 3H, Ar–H), 8.11 (d, J = 9.8 Hz, 1H, Ar–H), 7.59–7.53 (m, 3H, Ar–H + NH, D_2O exchangeable), 6.97 (d, J = 9.8 Hz, 1H, Ar–H), 2.01 (s, 3H, CH_3); ^{13}C NMR (100 MHz, DMSO-d_6) δ 174.3, 169.4, 154.8, 146.3, 144.4, 130.1, 129.1 (2C), 127.2 (2C), 125.2, 115.0, 21.0. Anal. calcd for $C_{13}H_{12}N_6O$ (268.28): C, 58.20; H, 4.51; N, 31.33; found, C, 58.47; H, 4.63; N, 31.50%.

*2.1.1.12 N′-(3-(4-methoxyphenyl)-[1,2,4]triazolo[4,3-b]pyridazin-6-yl)acetohydrazide (**6b**).* Brown solid: 75% yield m.p. 164–165 °C; IR (KBr, cm^{-1}) 3483, 3240 (2 NH), 3008 (CH aromatic), 2947, 2908 (CH aliphatic), 1685 (C=O), 1620 (C=N), 1577 (C=C); ^{1}H NMR (400 MHz, DMSO-d_6) δ 9.83 (s, 1H, NH, D_2O exchangeable), 8.39 (d, J = 8.4 Hz, 3H, Ar–H + NH, D_2O exchangeable), 8.10 (d, J = 9.8 Hz, 1H, Ar–H), 7.12 (d, J = 8.4 Hz, 2H, Ar–H), 6.96 (d, J = 9.8 Hz, 1H, Ar–H), 3.85 (s, 3H, OCH_3), 2.02 (s, 3H, CH_3); ^{13}C NMR (100 MHz, DMSO-d_6) δ 174.1, 169.5, 160.7, 154.7, 146.3, 144.1, 128.8 (2C), 125.3, 119.7, 114.5 (2C), 55.8, 21.1. Anal. calcd for $C_{14}H_{14}N_6O_2$ (298.31): C, 56.37; H, 4.73; N, 28.17; found, C, 56.70; H, 4.95; N, 28.41%.

2.2 Biological testing

The biological assays were completed using the previously disclosed methods, and they are included in the ESI;† antiproliferative activity screening by NCI,[41–45] MTT assay,[46] PI3K-Akt-mTOR pathway evaluation,[31] caspase-9 activity assay,[47] cell cycle analysis,[48] and apoptosis assay.[49]

2.3 *In silico* studies

2.3.1 Docking studies. Protein Data Bank was used to obtain the crystal structures of c-Met (PDB ID: 3CCN, resolution: 1.90 Å) and Pim-1 (PDB ID: 3BGQ, resolution: 2.00 Å). The MOE2014 program was implemented to achieve the docking investigation. First, water molecules were taken out of the crystal structures of c-Met and Pim-1. The proteins were then protonated and put through an energy-minimization process. The target proteins' active sites were consequently outlined. ChemBioDraw Ultra 14.0 was applied to construct the structures of the synthesized derivatives, compounds **I** and **IV** (used as reference standards), and the files were saved in MDL-SD format. The MOE program was used to open the file to display the protonated and energy-minimized 3D structures. Previously, the co-crystallized ligands were docked against the isolated pocket of the relevant enzymes' active sites to validate the docking procedure. The generated RMSD value demonstrated the process's viability. The tested compounds were finally docked using the dock option that was added to the computed window. Using the Triangle Matcher placement method and the

London dG scoring function, 30 docked poses were developed for each docked molecule.

2.3.2 Prediction of physicochemical, pharmacokinetic, and ADME properties. For the most efficacious compounds **4a** and **4g**, the physicochemical descriptors, pharmacokinetic characteristics, ADME, and drug-like nature were calculated using the SwissADME web tool, which is offered by the Swiss Institute of Bioinformatics (SIB). The structures were uploaded as SMILES notations to the web server for calculation.

3. Results and discussion

3.1 Chemistry

The new series of triazolo[4,3-*b*]pyridazine compounds **4a–g**, **5**, and **6a,b** is depicted in Scheme 1. First, 3-(2-arylidenehydrazinyl)-6-chloropyridazine derivatives **1a–c** were generated by refluxing 3-chloro-6-hydrazinopyridazine with the relevant aromatic aldehydes in absolute ethanol and glacial acetic acid.[38] Moreover, 6-chloro-3-arylidene-[1,2,4]triazolo[4,3-*b*]pyridazine derivatives **2a–c** were obtained by heating compounds **1a–c** under reflux at 80 °C in a mixture of ferric chloride and ethanol.[39] Compounds **2a–c** were heated under reflux at 80 °C with hydrazine hydrate in absolute ethanol to yield 6-hydrazinyl-3-arylidene-[1,2,4]triazolo[4,3-*b*]pyridazine derivatives **3a–c**.[40] New derivatives of 6-(2-arylidenehydrazinyl)-3-aryl-[1,2,4]triazolo[4,3-*b*]pyridazine (**4a–g**) were delivered by heating compounds **3a–c** under reflux at 80 °C with the appropriate aromatic aldehydes in absolute ethanol. Besides, 6-(3,5-dimethyl-1*H*-pyrazol-1-yl)-3-phenyl-[1,2,4]triazolo[4,3-*b*]pyridazine (**5**) was created by reacting compounds **3a** with acetylacetone in absolute ethanol.[50] Finally, [1,2,4]triazolo[4,3-*b*]pyridazine acetohydrazide compounds (**6a,b**) were obtained by refluxing acetic anhydride with the key intermediates **3a** and **3c** at 120 °C, respectively, in glacial acetic acid.

The retrieved derivatives' structures were supported by spectral and elemental data. The ^{1}H NMR spectra of compounds **4a–g** showed distinctive downfield singlet signals corresponding to the NH group of the hydrazone moiety, with δ values ranging from δ 11.36 to 12.15 ppm. As a stark example, the stretching bands in the IR spectrum for compound **4a** were located at 3425 cm^{-1} for the OH group and 3298 cm^{-1} for the NH group. Two downfield singlet signals, corresponding to the NH and OH groups, were noticed in the ^{1}H NMR spectrum of compound **4a** at δ = 11.65 and 9.97 ppm, respectively. On the other hand, the ^{1}H NMR spectrum of compound **5** demonstrated a sharp singlet peak at δ = 6.26 ppm representing the CH of the pyrazole ring, in addition to two strong up-field peaks at δ = 2.63 and 2.23 ppm corresponding to the two CH_3 groups attached to the pyrazole ring, which were confirmed by the ^{13}C NMR spectrum showing two peaks at δ = 14.8 and 13.8 ppm. Moreover, the ^{1}H NMR spectra of derivatives **6a,b** exhibited one singlet peak at δ = 9.72 ppm, corresponding to one of the NH of

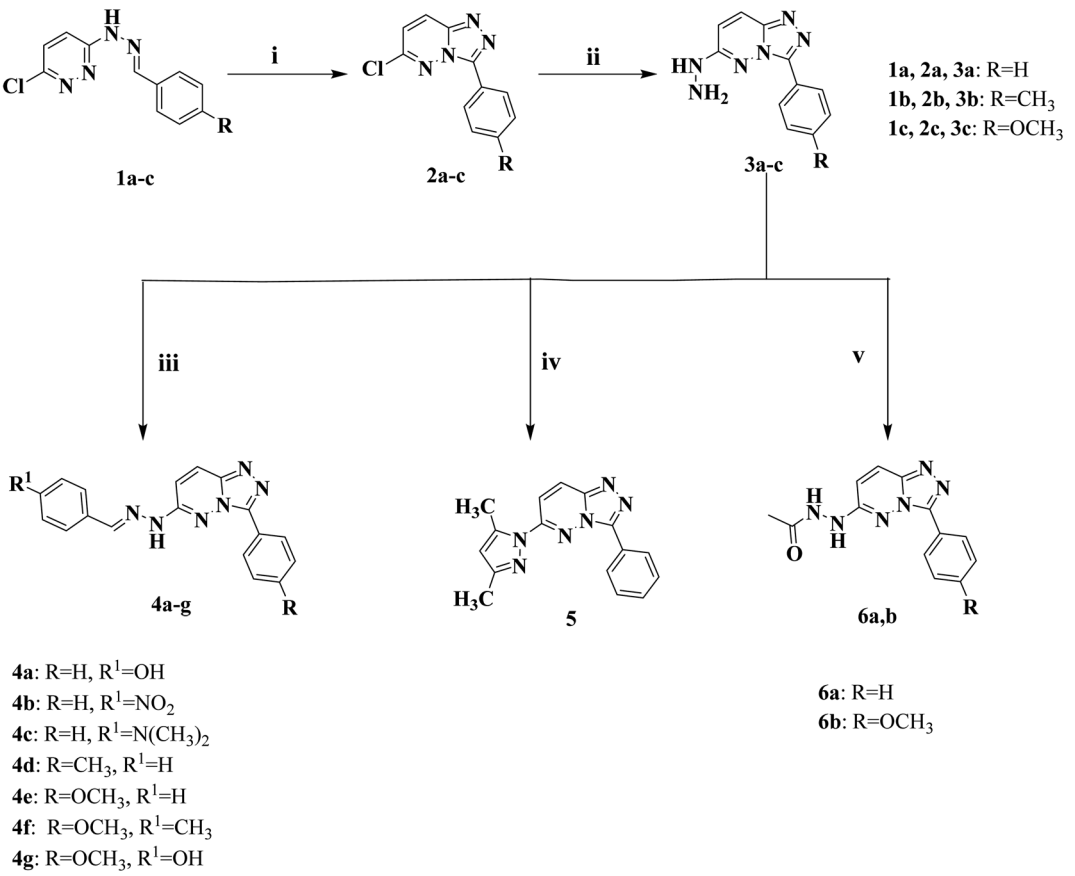

Scheme 1 Synthetic pathway of novel triazolo[4,3-*b*]pyridazine **4a–g**, **5**, and **6a,b**.

Table 1 GI% of the synthesized compounds **4a–g**, **5**, and **6a,b** against 60 tumor cell lines at 10 μM[ac]

Panel/cell lines										
Compounds	**4a**	**4b**	**4c**	**4d**	**4e**	**4f**	**4g**	**5**	**6a**	**6b**
Leukemia										
CCRF-CEM	**82.45**	—	—	—	—	—	**85.88**	—	—	—
RPMI-8226	**72.66**	—	—	19.37	—	—	**86.88**	—	—	—
NSC lung cancer										
A549/ATCC	24.99	—	—	—	21.90	66.62	41.49	—	—	—
EKVX	37.00	—	21.18	23.07	—	31.76	62.20	—	—	—
HOP-62	—	—	—	—	—	29.57	—	—	—	—
HOP-92	31.71	—	29.78	29.46	29.15	**81.11**	68.67	—	—	—
NCI-H226	—	—	—	—	42.42	45.38	22.48	—	—	—
NCI-H23	27.96	—	38.62	39.55	—	49.25	67.47	—	—	—
NCI-H322M	17.16	—	—	—	—	—	38.06	—	—	—
NCI-H460	25.61	—	18.89	31.51	—	48.83	55.73	—	—	—
NCI-H522	31.41	—	40.80	—	—	—	53.35	25.34	—	—
Colon cancer										
COLO-205	—	—	—	—	—	20.07	43.51	—	—	—
HCC-2998	—	—	—	—	—	20.85	**85.07**	—	—	—
HCT-116	37.12	—	—	—	—	21.17	**72.71**	—	—	—
HCT-15	34.22	—	19.56	30.81	—	50.02	**73.30**	—	—	—
HT29	—	—	—	—	—	17.40	—	—	—	—
KM12	46.62	—	28.28	42.77	—	31.89	**71.51**	—	—	—
SW-620	—	—	—	—	—	—	32.85	—	—	—
CNS cancer										
SF-268	34.95	—	57.96	42.23	—	40.91	64.19	—	—	—
SF-295	16.99	—	—	47.66	—	43.09	56.41	—	—	—
SF-539	43.13	—	—	19.19	17.17	38.74	63.61	—	—	—
SNB-19	21.93	—	30.50	—	17.10	—	32.46	—	—	—
SNB-75	25.31	—	65.40	**>100**	62.97	**>100**	46.38	—	—	—
U251	—	—	24.58	24.9	22.16	55.13	32.41	—	—	—
Melanoma										
LOX IMIV	51.37	—	62.55	52.47	29.87	**76.27**	**>100**	22.70	—	—
MALME-3M	—	—	—	—	—	—	35.83	—	—	—
M14	—	—	—	32.66	—	16.52	43.64	—	—	—
MDA-MB-435	37.50	—	—	23.87	—	35.32	54.20	—	—	—
SK-MEL-2	—	—	—	—	—	—	26.79	—	—	—
SK-MEL-28	—	—	—	—	—	—	30.86	—	—	—
UACC-257	—	—	—	—	—	—	17.70	—	—	—
UACC-62	16.98	—	—	—	—	—	41.19	—	—	—
Ovarian cancer										
IGROV1	21.21	—	—	—	—	—	60.66	—	—	—
OVCAR-3	35.66	—	34.65	69.65	—	**84.42**	62.40	—	—	—
OVCAR-4	26.85	—	41.36	30.86	—	63.09	52.11	—	—	—
OVCAR-5	—	—	—	—	—	—	—	—	—	—
OVCAR-8	25.02	—	57.57	—	34.25	58.61	54.60	—	—	—
NCI/ADR-RES	41.13	—	55.19	15.93	30.10	**74.21**	**73.98**	23.93	—	—
SK-OV-3	—	—	—	—	—	20.16	—	—	—	—
Renal cancer										
786-0	46.01	—	18.27	—	—	43.09	**77.10**	—	—	—
A498	—	—	—	—	—	—	—	—	—	—
ACHN	25.31	—	21.61	—	—	41.02	56.52	—	—	—
CAKI-1	57.00	—	32.25	16.69	—	45.37	**78.54**	25.28	—	—
RXF 393	22.59	—	15.29	—	—	37.84	57.34	—	—	—
SN12C	39.51	—	—	—	—	23.07	57.71	—	—	—
TK-10	30.62	—	—	—	—	17.28	61.05	—	—	—
UO-31	49.79	—	18.89	15.52	—	66.50	69.74	**>100**	—	—

Table 1 (*Contd.*)

Panel/cell lines										
Compounds	**4a**	**4b**	**4c**	**4d**	**4e**	**4f**	**4g**	**5**	**6a**	**6b**
Prostate cancer										
PC-3	27.08	—	18.94	—	—	27.83	59.52	—	—	—
DU-145	—	—	26.64	24.06	—	60.93	48.11	—	—	—
Breast cancer										
MCF7	**71.51**	—	34.47	52.06	28.54	42.84	**86.77**	—	—	—
MDA-MB-231/ATCC	—	—	—	—	34.41	34.65	39.44	—	—	—
HS 578T	—	—	33.19	53.45	17.35	**70.93**	53.18	—	—	—
T-47D	16.17	—	22.66	—	—	24.01	54.64	—	—	—
MDA-MB-468	30.50	—	—	—	—	—	51.76	—	—	—
Mean inhibition[b]	**29.08**	<0	17.68	18.27	7.15	34.83	**55.84**	<0	—	<0

[a] — GI% is below 15%. [b] Mean inhibition: GI% values over all NCI-60 cell lines. [c] Bold: GI% from 70 to 100%.

the acetohydrazide group in addition to a strong singlet peak at $\delta = 2.01$ ppm in **6a** and 2.02 ppm in **6b** representing the CH_3 group of the acetohydrazide part. The previously mentioned data were confirmed by the IR spectra, which showed two bands at the range of 3483–3232 cm^{-1} for the two NH groups and 1685 cm^{-1} for the amidic C=O group in **6a,b**, in addition to the ^{13}C NMR spectra, which displayed characteristic peaks at $\delta =$ 174.3 ppm in **6a** and 174.1 ppm in **6b** corresponding to the amidic C=O and a peak at $\delta = 21.0$ ppm corresponding to the CH_3 groups in **6a,b**.

3.2 Biological evaluation

3.2.1 *In vitro* antiproliferative assay on NCI 60-cell lines. The National Cancer Institute (USA) evaluated the antiproliferative activity of ten newly synthesized triazolo[4,3-*b*]pyridazine derivatives (**4a–g**, **5**, and **6a,b**) as part of the developmental therapeutic program (DTP).[41–45] One dose (10 μM) of the substances was evaluated against 60 human tumor cell lines. Different antiproliferative effects of the compounds are shown in Table 1 as growth inhibition percentages (GI%). The *p*-methoxy-*p*-hydroxy-triazolopyridazine hydrazone derivative **4g** was the most active compound against various numerous cancer cell lines, with a mean growth inhibition percent of 55.84 showing strong antiproliferative activity against 10 cell lines, including leukemia (CCRF-CEM with GI% 85.88 and RPMI-8226 with GI% 86.88); colon cancer (HCC-2998 with GI% 85.07, HCT-116 with GI% 72.71, HCT-15 with GI% 73.30, and KM12 with GI% 71.51); ovarian cancer (NCI/ADR-RES with GI% 73.98); renal cancer (786-0 with GI% 77.10, CAKI-1 with GI% 78.54), and breast cancer (MCF7 with GI% 86.77).

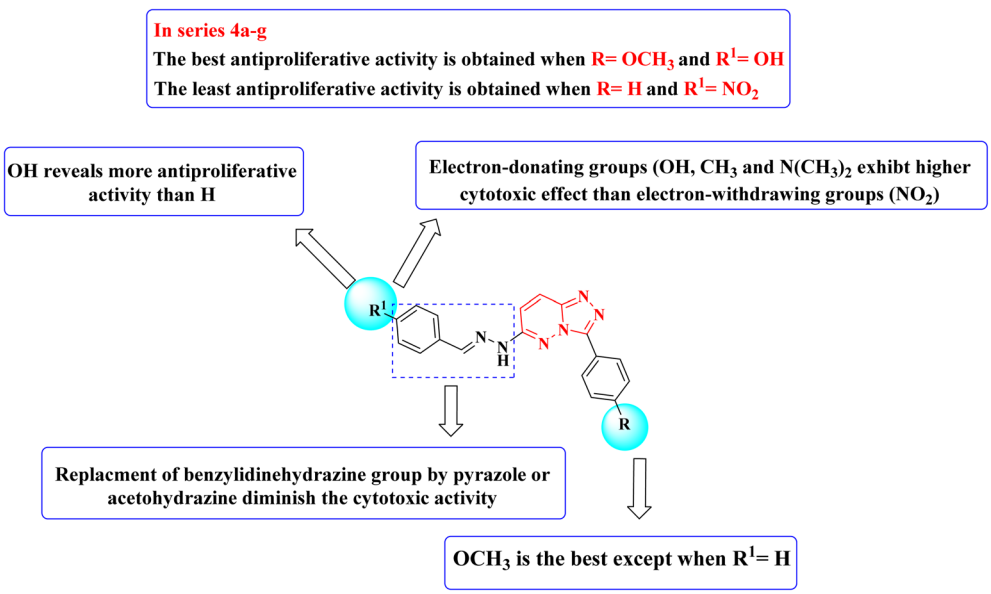

Fig. 3 Structure–activity relationship (SAR) of the synthesized triazolo[4,3-*b*]pyridazine derivatives.

In addition, it displayed moderate activity against 35 cell lines with a GI% range between 30.86 and 69.74 and lethal activity against melanoma LOX IMIV. Substituting the *p*-hydroxy group in **4g** with the *p*-methyl group and maintaining the *p*-methoxy group yielded the derivative **4f** with a mean growth inhibition percent of 34.83. Compound **4f** demonstrated strong antiproliferative activity against NSC lung cancer (HOP-92 with GI% 81.11), ovarian cancer (OVCAR-3 with GI% 84.42 and NCI/ADR-RES with GI% 74.21), and breast cancer (HS 578 T with GI% 70.93).

Moreover, it produced moderate activity against 22 cell lines with GI% ranging from 31.76 to 66.62 and lethal activity against the CNS cancer SNB-75. On the other hand, compound **4a**, which resulted from the removal of the *p*-methoxy group of **4g**, displayed a mean growth inhibition percent of 29.08 and displayed strong anticancer activity against leukemia (CCRF-CEM with GI% 82.45 and RPMI-8226 with GI% 72.66) and breast cancer (MCF7 with GI% 71.51) as well as moderate activity against 18 cancer cell lines with GI% ranging from 30.62 to 57.00. The absence of both *p*-methoxy and *p*-hydroxy substituents resulted in derivatives with low to moderate cytotoxic activity (compound **4b**). Replacement of the hydrazone moiety with either a pyrazole ring (compound **5**) or acetohydrazide group (derivatives **6a,b**) resulted in compounds with demolished cytotoxicity, which confirmed the importance of the hydrazone part in the anticancer activity of the synthesized compounds.

Structure–activity relationship studies (SAR) were studied for the synthesized triazolo[4,3-*b*]pyridazine derivatives **4a–g**, **5**, and **6a,b**. The percentage inhibition pattern for the compounds showed that the benzylidene group is essential for showing any degree of antiproliferative activity, and methoxy substitution on the phenyl ring shows the best cytotoxicity except for the unsubstituted benzylidene derivative. Moreover, hydroxy substitution on the benzylidene ring displayed optimal antiproliferative activity. Electron-donating groups on the benzylidene moiety were required to show cytotoxic activity, while substitution with electron-withdrawing groups resulted in demolished cytotoxicity, as shown in Fig. 3.

3.2.2 MTT assay and selectivity index (SI) calculation. Based on the NCI single-dose screening growth inhibition percentages, a preliminary test was conducted to estimate compounds **4a** and **4g** antiproliferative activity against the breast cancer cell line MCF7. The Mosmann's MTT colorimetric assay protocol was followed.[46] Moreover, the experiments were conducted using staurosporine as a reference drug. Based on the outcomes, growth inhibitory concentration (IC_{50}) values were calculated, indicating the concentration inhibited 50% of cell growth after 72 h (Table 2). According to cytotoxicity studies, compound **4g** had the greatest antiproliferative effect on the MCF7 breast cell lines, followed by compound **4a** with IC_{50} = 0.56 ± 0.03 and 2.97 ± 0.18 μM, respectively, compared to the IC_{50} of staurosporine of 8.04 ± 0.48 μM. In addition, chemotherapeutic agents have undesirable side effects on normal cells. This is attributed to the undistinguishable cytotoxicity of anticancer drugs. Therefore, we assessed the effect of compounds **4a** and **4g** on the human mammary epithelial cell line (MCF10a) as a normal breast cell. Besides, the selectivity index (SI) was calculated to measure the degree of toxicity of these derivatives on normal breast cell lines. Table 2 shows the results of SI against normal cells. The SI was calculated by comparing the cytotoxicity (IC_{50}) of the normal breast cell line (MCF10a) with the breast cancer cell line (MCF7). The results revealed that compound **4g** was the most selective to breast cancer cell line (MCF7) with an IC_{50} of 10.70 ± 0.56 μM and SI of 19.11. Compound **4a** scored an IC_{50} value of 15.80 ± 2.92 μM for MCF10a with SI = 5.32 compared to staurosporine, which scored an IC_{50} value of 18.32 ± 8.03 μM with SI = 2.28.

3.2.3 Enzyme inhibitory assays. As compounds **4a** and **4g** exhibited promising cytotoxic activity, their inhibitory nature as dual c-Met and Pim-1 kinases was examined *in vitro* as part of our attempts to understand the mechanism of these compounds. The **4a** and **4g** profiles against c-Met and Pim-1 kinases were estimated using standard assay procedures. The results are presented in Table 3 and Fig. 4 as the 50% inhibition concentration value (IC_{50}) derived from the concentration inhibition response curve compared with staurosporine. Compound **4g** inhibited both c-Met and Pim-1 kinases with IC_{50} of 0.163 ± 0.01 and 0.283 ± 0.01 μM compared to staurosporine, which showed IC_{50} of 0.277 ± 0.017 and 0.468 ± 0.02 μM with both c-Met and Pim-1 kinases, respectively. On the other hand, compound **4a** showed lower inhibition against c-Met and Pim-1 kinases with IC_{50} of 0.452 ± 0.028 and 0.712 ± 0.03 μM, respectively. According to these biological findings, compounds can dually inhibit c-Met and Pim-1 kinases associated with its antiproliferative activity.

3.2.4 Evaluation of the PI3K-Akt-mTOR pathway. To determine the molecular mechanism by which compound **4g** triggers apoptosis in cancer cells and identify this pathway's target, we examined the PI3K-Akt-mTOR pathway. Several biological mechanisms are part of the PI3K-Akt-mTOR pathway

Table 2 *In vitro* cytotoxicity IC_{50} of compounds **4a** and **4g** against breast cancer cell line MCF7 and normal cell line MCF-10a compared to staurosporine

	Cytotoxicity IC_{50} μM ± SD[a]		
Compounds	MCF7	MCF10a	Selectivity index
4a	2.97 ± 0.18	15.80 ± 2.92	5.32
4g	0.56 ± 0.03	10.70 ± 0.56	19.11
Staurosporine	8.04 ± 0.48	18.32 ± 8.03	2.28

[a] IC_{50} is presented as a mean of 3 experiments.

Table 3 IC_{50} values of compounds **4a** and **4g** on c-Met and Pim-1 enzymes compared to staurosporine as a reference drug

Compounds	c-Met IC_{50}[a] (μM ± SD)	Pim-1 IC_{50}[a] (μM ± SD)
4a	0.452 ± 0.028	0.712 ± 0.03
4g	0.163 ± 0.01	0.283 ± 0.01
Staurosporine	0.277 ± 0.017	0.468 ± 0.02

[a] IC_{50} is presented as the mean of three independent experiments.

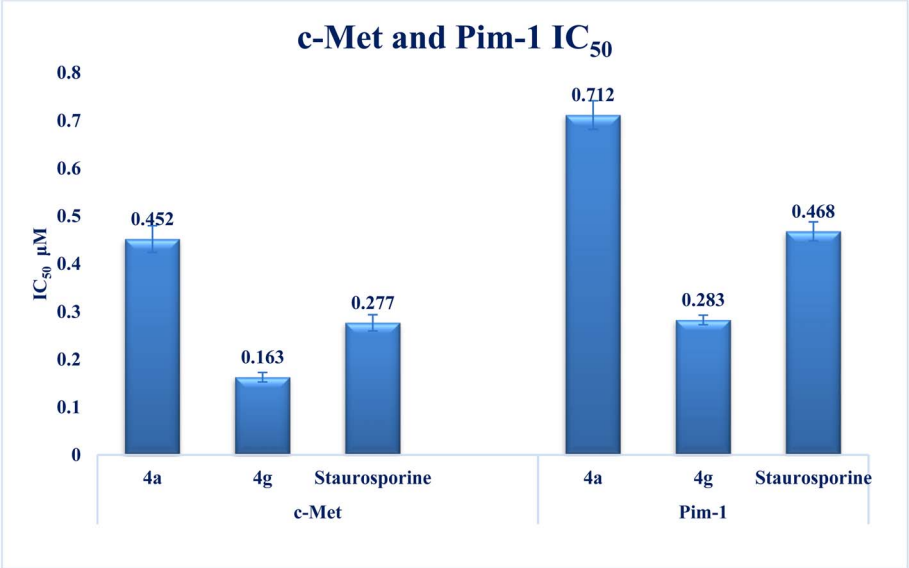

Fig. 4 Graph showing IC_{50} inhibition of both c-Met and Pim-1 kinases of compounds **4a** and **4g** in comparison to staurosporine.

that contribute to the spread of cancer, including cell division, migration, angiogenesis, and metastasis. To assess the capability of compound **4g** in inhibiting phosphorylation within the PI3K-Akt-mTOR pathway in breast cancer cell lines MCF7, it was evaluated at its IC_{50} value, which was determined to be 0.56 µM. Compound **4g** was found to strongly inhibit PI3K phosphorylation by 55.5% compared to MCF7 cells that were not treated (Fig. 5). As compared with staurosporine, PI3K phosphorylation was inhibited by 34.6%. Moreover, compound **4g** suppressed the phosphorylation of AKT and mTOR by 76.6% and 74.6%, respectively, compared to staurosporine, which inhibited *p*-AKT and *p*-mTOR by 69.02% and 71.16%, respectively. These findings demonstrated that compound **4g** down-regulated PI3K, Akt, and mTOR protein phosphorylation.

3.2.5 Caspase 9 activity determination of compound 4g. A caspase-9 assay was then conducted using the most active compound, **4g**, to detect whether this compound could induce apoptosis in breast cancer MCF7 cells compared to control untreated cells and staurosporine as the reference drug.[47] Compound **4g** significantly boosted the level of apoptotic caspase-9 by 11.6-fold, while staurosporine increased its level by 7.19-fold (Fig. 6). This suggested that compound **4g** triggered apoptosis through caspase-9 activation.

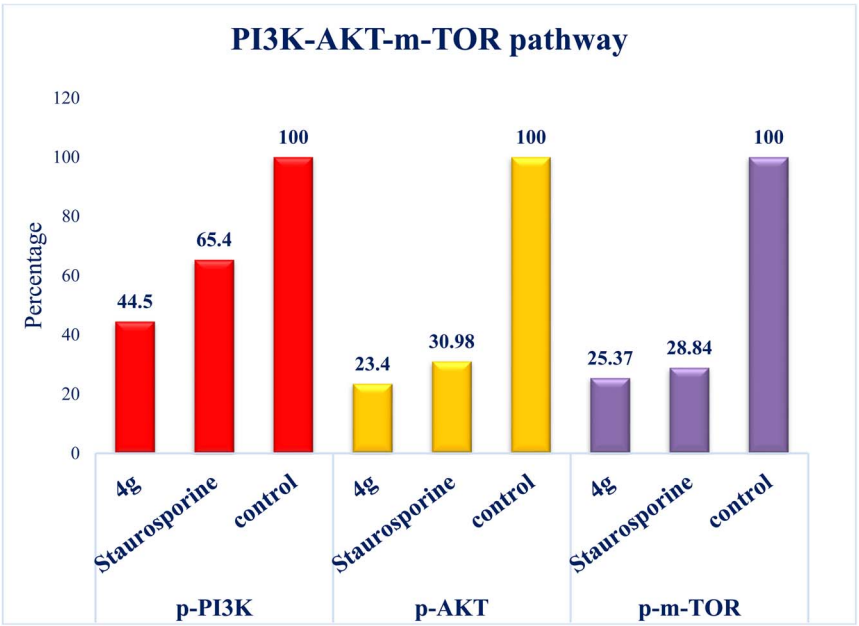

Fig. 5 The plot shows the down-regulation of phosphorylation of PI3K-Akt-mTOR pathway in breast cell line MCF7 cells following the application of compound **4g**, *versus* staurosporine and untreated control cells.

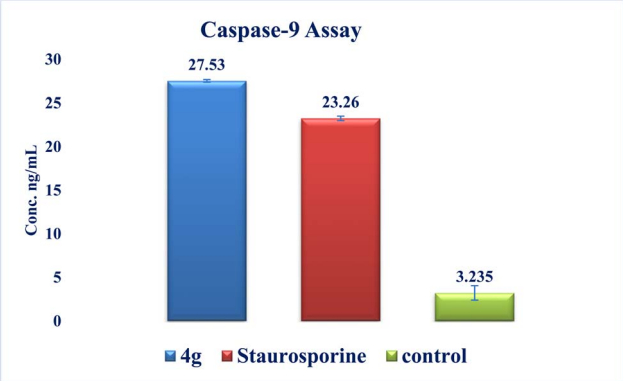

Fig. 6 Graphical representation for active caspase-9 assays of compound **4g** compared to staurosporine as a control.

3.2.6 Analysis of cell cycle. An antitumor agent can induce apoptosis by activating signaling pathways in the cell, which can cause an arrest in a particular cell cycle phase. An analysis of the cell cycle was conducted through flow cytometry, which monitors cell growth in different cell cycle phases (pre-G1, G1, S, and G2/M) to distinguish between cells within different cell cycle phases.[48] An investigation into the cell cycle arrest phase in the MCF7 breast cancer cell line was carried out by studying the effect of the most active compound, **4g**, on cell cycle progression, and DMSO was used as a negative control. Fig. 7 shows the effects of compound **4g** on the cell population of MCF7 cells in different cell phases when treated with its IC_{50} value (0.56 μM). A drop in the cell population of MCF7 cells exposed to compound **4g** at the G0/G1 and G2/M phases was recorded at 10.48% (from 59.14% to 52.94%) and 46.84% (from 7.778% to 4.13%), respectively. Additionally, in comparison with the control (DMSO), a marked increase in the proportion of cells in the S phase was observed (1.29-fold). Based on the results of this study, it appears that the target derivative **4g** has caused an arrest in the proliferation of MCF7 cells in the S phase.

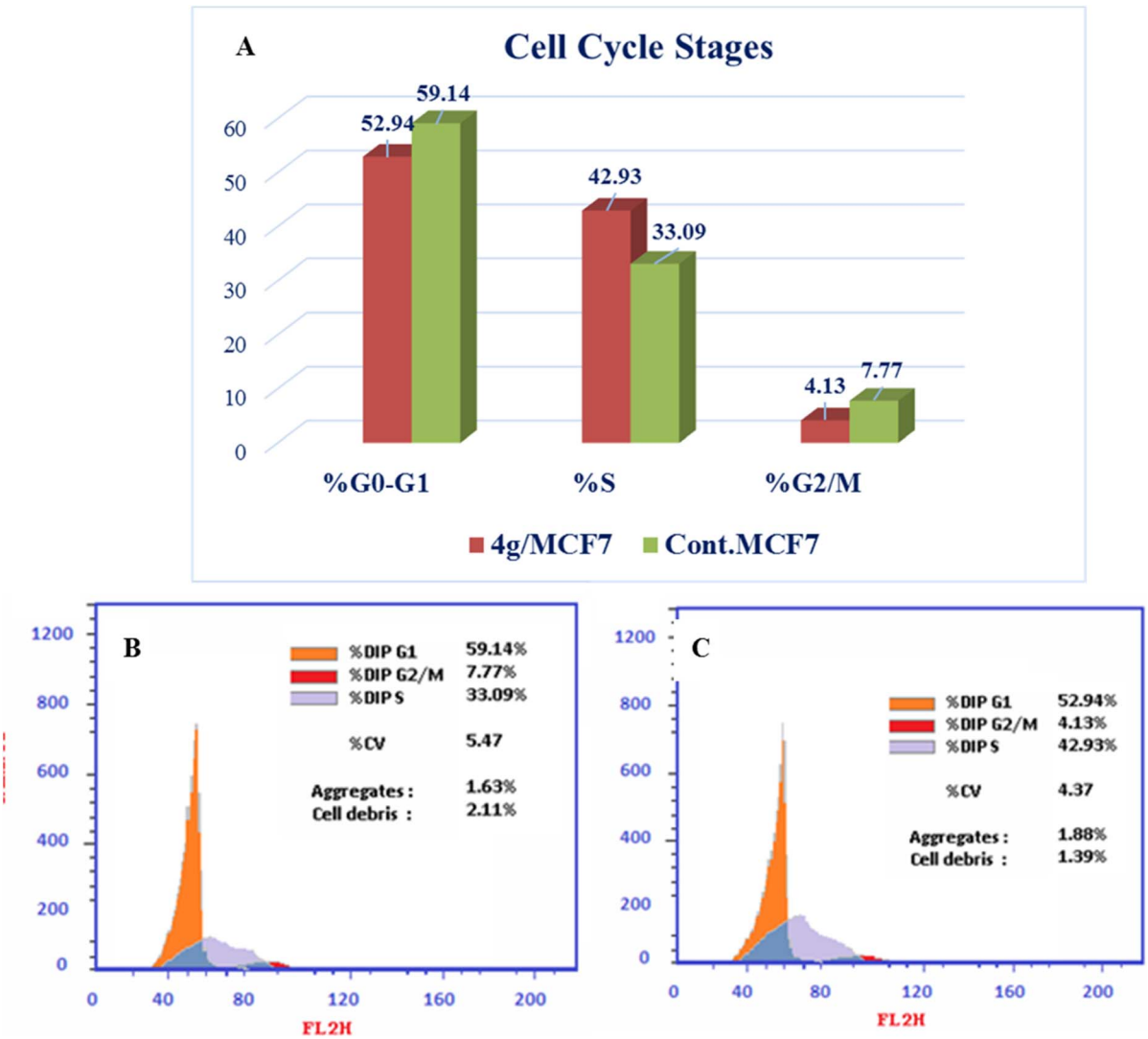

Fig. 7 Cell cycle analysis in the breast MCF7cell line. (A) Graphical diagram for the distribution of cell cycle analysis in treated and control cells. (B) Control MCF7. (C) Treatment with compound **4g**.

Table 4 After treatment with compound **4g**, the distribution of apoptotic cells was determined using the annexin V/PI dual staining assay in MCF7 cells

	Apoptosis			
Compound	Total	Early	Late	Necrosis
4g/MCF7	48.56	25.16	18.13	5.27
Cont. MCF7	1.64	0.36	0.18	1.1

3.2.7 Evaluation of apoptosis by annexin V. The most important mechanism of action of anticancer agents is the induction of apoptosis in cancer cells. Dual staining for annexin-V and propidium iodide (PI) permits discrimination between different apoptotic stages of cells.[49] The annexin-V/PI dual-staining method was employed for cytometric analysis to differentiate between apoptosis and necrosis modes of cell death in MCF7 cells in response to the most potent compound, **4g**. As shown in Table 4 and Fig. 8, after 24 h of exposure to compound **4g** at its IC_{50} concentration (0.56 μM), a decrease in the percentage of MCF7 cells that survived was observed. There was an increase in the percentage of apoptotic cells in the early apoptosis phase from 0.36% to 25.16% and a significant increase in the late apoptosis phase from 0.18% to 18.13%. It corresponds to a 29.61-fold increase in the percentage of total apoptosis (from 1.64% to 48.56%) compared to the control. The outcomes of this study lead to the conclusion that the antiproliferative effects exhibited by the target derivative **4g** are attributed to its inherent apoptotic properties.

3.3 *In silico* studies

3.3.1 Molecular docking studies. Compound **I** was used as a reference ligand in molecular docking studies against c-Met (PDB ID: 3CCN) to look at potential binding interactions with the target receptor. In this study, we also considered the binding free energy (G) between the docked molecules and the active sites in addition to the appropriate binding mode. The reported binding mode against c-Met involves important interactions with several crucial amino acid residues, including a hydrogen bond interaction with Met 1160 and a stack interaction with Tyr1230. The binding free energies are presented in Table 5. To validate the accuracy of the docking process, the docking procedures were initially executed solely for the co-crystallized ligand within the active pocket. The created RMSD value between the docked molecule's new position and the initial one is 1.29. This demonstrated that the docking procedure was valid (Fig. 9). The binding mode of compound **I** with c-Met as a reference ligand revealed a binding free energy of -9.45 kcal mol^{-1}.

One hydrogen bond was created between the amino acid residue Asp1222 and the hydrogen bond acceptor (N1 of the triazole ring). Due to the hydrophobic interaction, two hydrophobic bonds were formed between Tyr1230 and the triazolopyridazine core group. Additionally, the phenol moiety

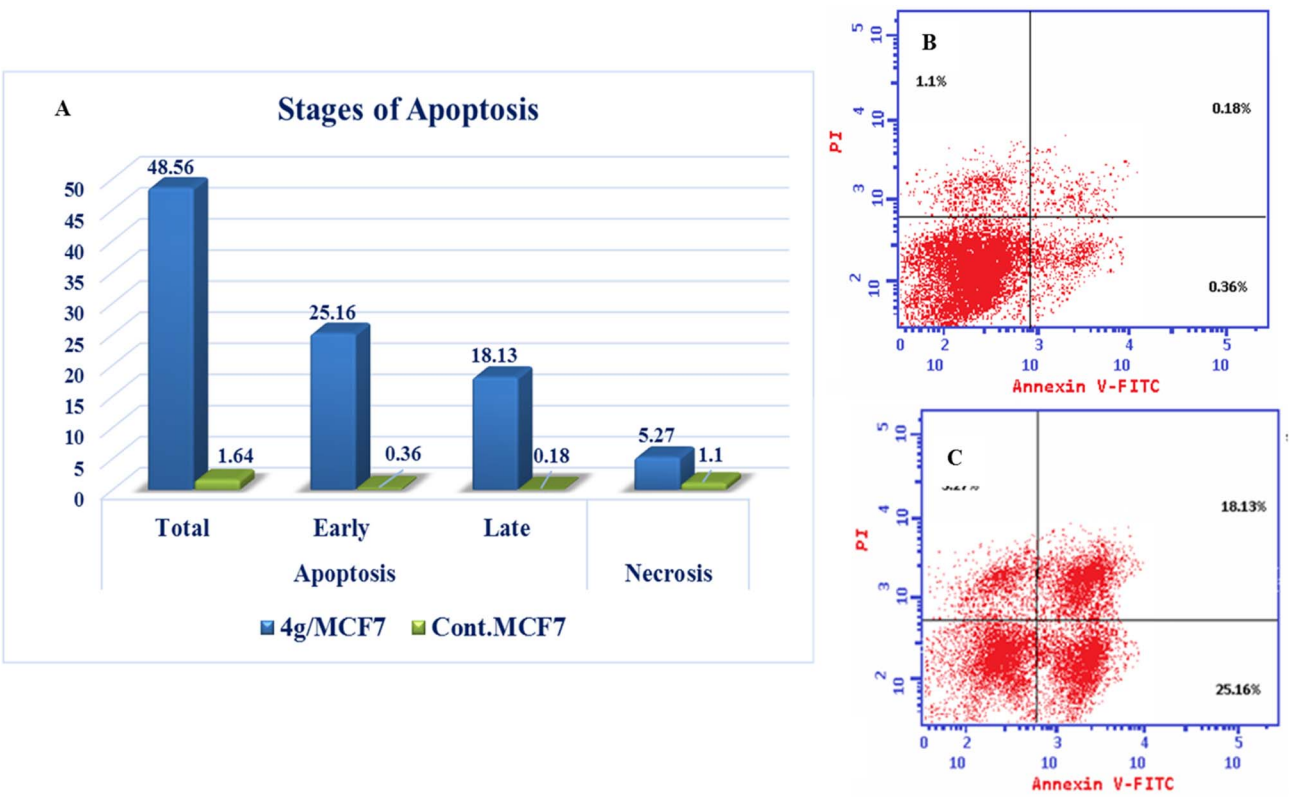

Fig. 8 Annexin V positive staining in MCF7 breast cells after compound **4g** treatment. (A) Diagram showing the apoptosis and necrosis in treated and control cells. (B) Control MCF7. (C) Treatment with compound **4g**.

Table 5 Table illustrating the docking energy scores (S) in kcal mol^{-1}, the amino acids, and their interaction types, and the distance of the active compounds **4a** and **4g** within the c-Met and Pim-1 active sites

Compound/enzyme	S (kcal mol^{-1})	Amino acids	Interaction types	Distance (Å)
4a/c-Met	−7.49	Ile1084	π–H	4.49
		Tyr1230	π–π	3.59
		Met1160	HB acceptor	2.76
		Pro1158	HB donor	2.70
4g/c-Met	−8.55	Ile1084	π–H	4.24
		Ile1084	π–H	3.93
		Met1160	HB acceptor	3.11
		Met1160	HB acceptor	3.20
I/c-Met	−9.45	Tyr1230	π–H	4.08
		Val1092	π–H	4.01
		Tyr1230	π–π	3.95
		Tyr1230	π–π	3.73
		Met1160	HB acceptor	3.06
		Asp1222	HB acceptor	3.40
		Val1092	π–H	4.15
		Met1211	π–H	3.68
4a/Pim-1	−7.97	Lys67	HB acceptor	3.42
		Lys67	HB acceptor	3.44
		Val52	π–H	3.91
		Val52	π–H	4.27
		Val52	π–H	3.99
		Ile185	π–H	4.08
		Ile185	π–H	4.09
		Phe49	π–π	3.73
		Asp128	HB donor	3.09
4g/Pim-1	−8.24	Lys67	HB acceptor	3.27
		Val52	π–H	4.23
		Val52	π–H	4.01
		Asp128	HB donor	3.17
		Asp131	HB donor	3.25
IV/Pim-1	−9.05	Lys67	HB acceptor	3.02
		Lys67	HB acceptor	3.11
		Val52	π–H	4.56
		Ile185	π–H	4.04
		Ile185	π–H	4.26
		Ile185	π–H	4.46
		Phe49	π–π	3.95

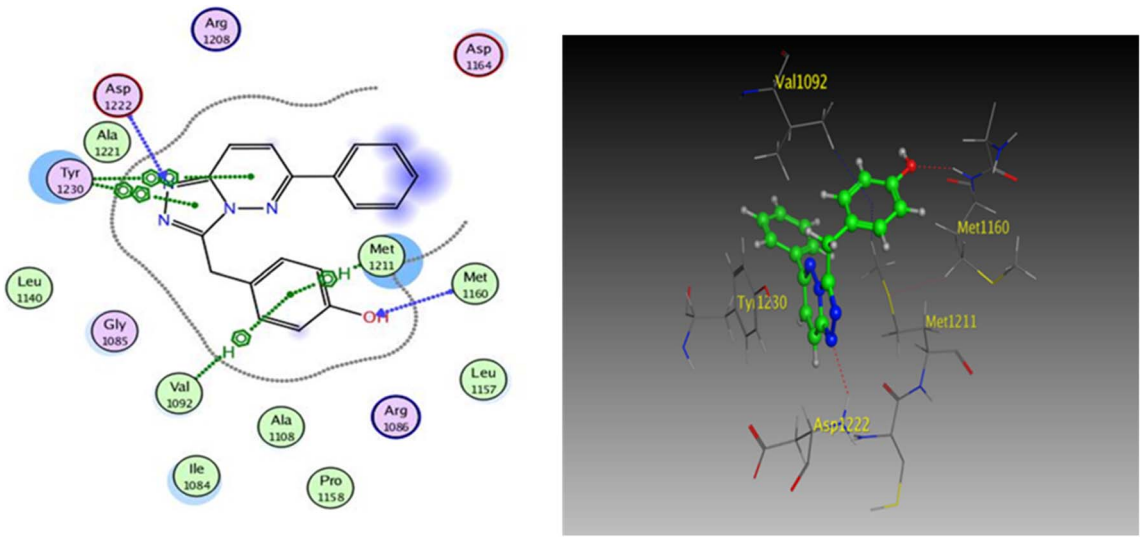

Fig. 9 2D and 3D diagrams of compound **I** interactions with c-Met (PDB ID: 3CCN) (in 3D figure hydrogen bonds are represented in red and hydrophobic interactions in blue).

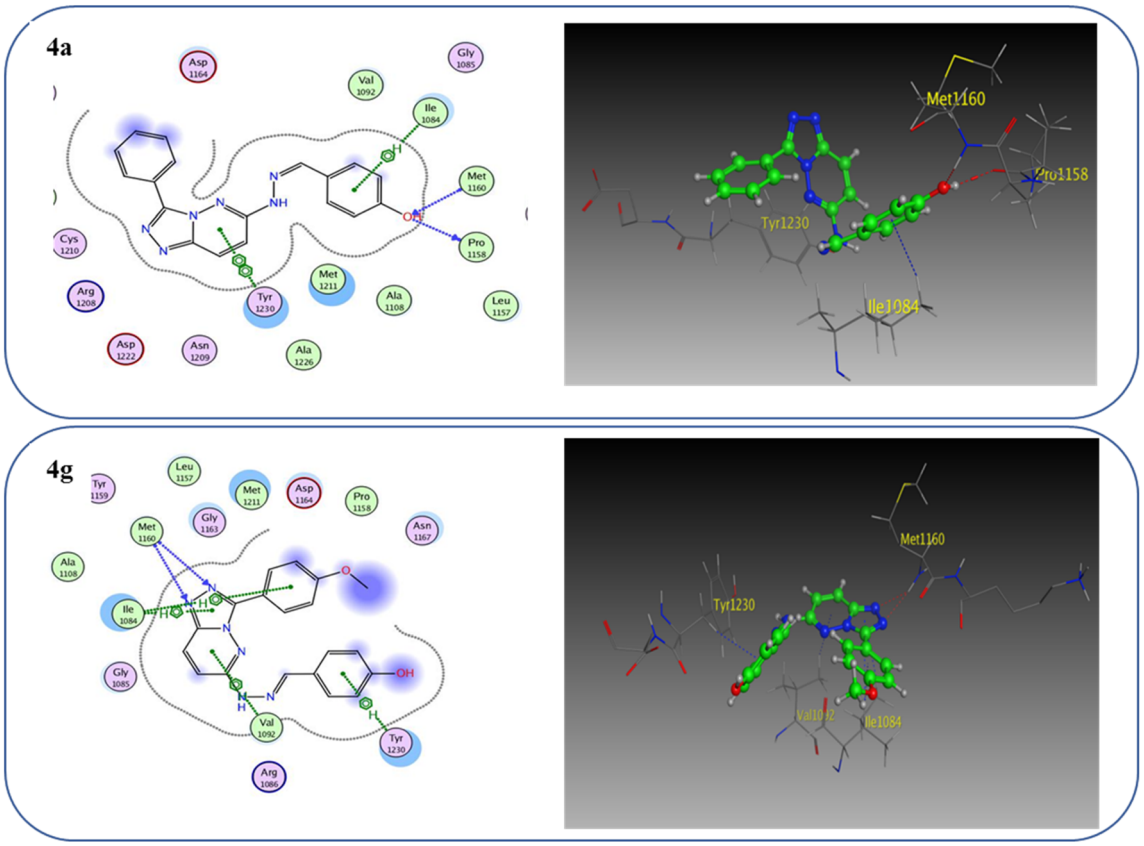

Fig. 10 2D and 3D interaction diagrams of derivative **4a** and **4g** interactions with c-Met in 2D and 3D diagrams.

formed two hydrophobic interactions with Met1211 and Val1092 through the phenyl ring, forming a hydrogen bond *via* its O with Met1160. These results closely match the described data.[28] Similar to the vital interactions of compound **I**, the target molecules interacted with the active site of c-Met in a manner that demonstrated binding mode. The binding affinity of compound **4a** was −7.49 kcal mol^{-1}. The critical amino acid residue Tyr1230 formed a π–π stack interaction with the triazolopyridazine core. The terminal phenol group formed a bifurcated hydrogen bond interaction with Met1160 and Pro1158 through the HBA/HBD (OH) substituent and was incorporated in a hydrophobic interaction with Ile1084 through

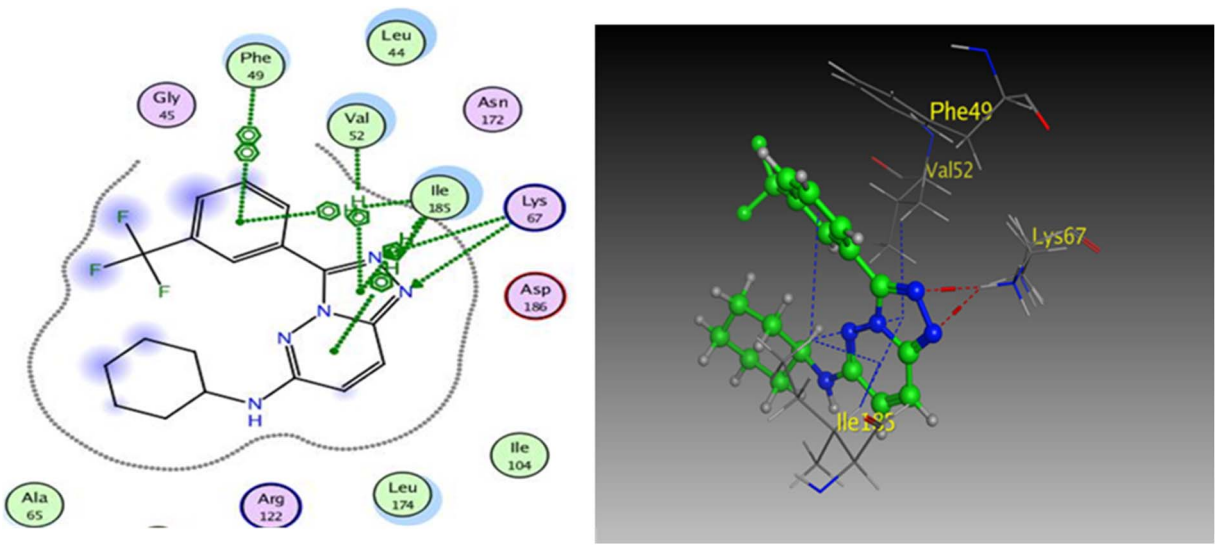

Fig. 11 2D and 3D diagrams of compound **IV** interactions with Pim-1 (PDB ID: 3BGQ).

its phenyl group. Compound **4g** exhibited binding energy up to −8.55 kcal mol^{-1}. First, the N_1 and N_2 of the triazolo ring functioned as hydrogen bond acceptors and formed two hydrogen bonds with Met1160 which may contribute to its potency. Second, the phenoxy side chain's triazolopyridazine core and phenyl moiety formed three hydrophobic bonds with Ile1084 and Val1092. Third, the phenyl group of the phenol moiety formed a π–π stack interaction with the crucial amino acid residue Tyr1230 (Fig. 10).

To prove the dual action of our derivatives, a docking study was carried out on Pim-1 (PDB ID 3BGQ) using compound **IV** as a reference ligand.[29] The docking process was validated, and the ligand achieved −9.05 kcal mol^{-1} binding free energy with an RMSD value of 1.22. There were two crucial interactions, a hydrogen bond with Lys67 and a hydrophobic interaction with Val52 amino acid residues, besides other hydrophobic interactions (Fig. 11). It was found that compound **4a** bound to the active pocket with a binding energy of −7.97 kcal mol^{-1} through three hydrogen bond interactions, two with Lys67 *via* N_1 of the triazole moiety as HBA, and the third one between the Asp128 residue and the OH of the phenol ring as HBD. In addition to the hydrogen bonds, the derivative **4a** formed many hydrophobic interactions with Val52, Phe49, and Ile185 amino acids. In the same context, compound **4g** was effectively linked to the active pocket through different types of hydrogen bonds with Lys67, Asp128, and Asp131, which could be the reason for its potency, besides two hydrophobic interactions with Val52 (Fig. 12). The binding energy with the receptor was −8.24 kcal mol^{-1}.

3.3.2 Prediction of physicochemical, pharmacokinetic, and ADME properties. The most potent triazolopyridazine derivatives, **4a** and **4g**, are available from the Swiss Institute of Bioinformatics (SIB) using the SwissADME online tool, which is used to calculate the physicochemical properties, predict the pharmacokinetic properties, and determine how drug-like they are.[51] By examining their pharmacokinetic characteristics and biological efficacy, compounds **4a** and **4g** are promising candidates. The ESI† shows the data that has been condensed. The compounds **4a** and **4g** that were submitted displayed no BBB permeability, a predicted WLOGP value of 2.75 and 2.76, respectively, were moderately water-soluble, had a high GIT absorption rate (high oral bioavailability), and did not exhibit any expected CNS side effects. Fig. 13 shows the BOILED-egg graph for the proposed compounds **4a** and **4g** of the WLOGP *vs.* TPSA (Topological Polar Surface Area).[52] In the region of human intestinal absorption (HIA) with no BBB permeability, compounds **4a** and **4g** have been identified.

Additionally, this graph demonstrates that compounds **4a** and **4g** are not P-glycoprotein substrates (PGP), which means they are immune to the transporter's efflux system, which many

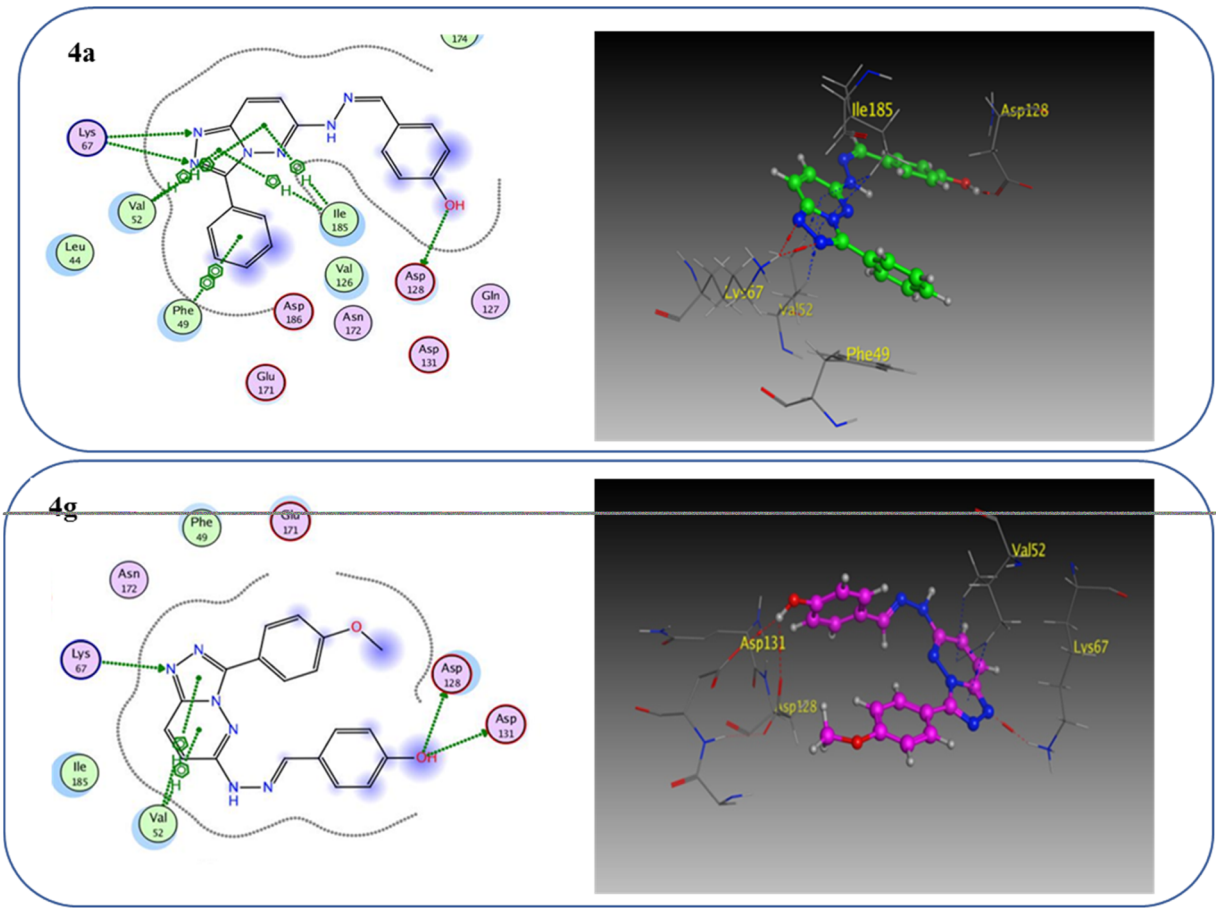

Fig. 12 2D and 3D diagrams of compound **4a** and **4g** interactions with Pim-1.

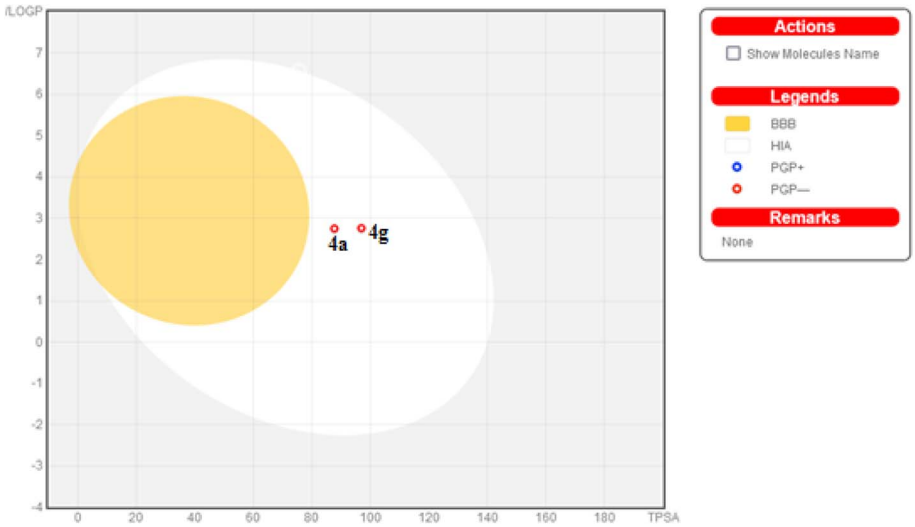

Fig. 13 Predicted boiled-egg plot from SwissADME online web tool for compounds **4a** and **4g**.

tumor cell lines use as a mechanism for drug resistance. Compounds **4a** and **4g**, according to the SwissADME online web tool, fulfill the criteria for drug-likeness established by the major pharmaceutical companies due to their high molecular weight and log *P*. According to the computational analysis of the physicochemical and pharmacokinetic properties, compounds **4a** and **4g** have promising pharmacokinetic and biological efficacy characteristics.

4. Conclusion

New series of triazolo[4,3-*b*]pyridazine derivatives **4a–g**, **5**, and **6a,b** were successfully created. The NCI-60 human cancer cell line panel was used to screen the synthesized compounds' anticancer activity. Compounds **4a** and **4g** demonstrated extensive antiproliferative activity on various cell lines. The most effective derivatives against the breast cancer cell line MCF7 were compound **4a** and compound **4g**, with IC_{50} values of 2.97 ± 0.18 and 0.56 ± 0.03 μM, respectively. While compound **4g** displayed higher inhibition on c-Met with an IC_{50} of 0.163 ± 0.01 and Pim-1 with an IC_{50} of 0.283 ± 0.01 μM, compound **4a** displayed lower dual inhibition of c-Met and Pim-1 with IC_{50} values of 0.452 ± 0.028 and 0.712 ± 0.03 μM, respectively. According to an annexin V-FITC/PI assay, the most potent compound, **4g**, significantly increased the early and late apoptosis phases in MCF-7 cells, respectively, from 0.36 to 25.16% and from 0.18 to 18.13%. An increase of 11.6-fold in the amount of apoptotic caspase-9 served as additional support for this evidence. In addition, cell cycle analysis results revealed that derivative **4g** ceased the proliferation of MCF-7 cancer cells in the S phase. These findings confirm **4g**'s cytotoxic potential and could make it a candidate for additional biological testing. According to the findings of a molecular docking study, the binding pattern of compound **4g** is consistent with its dual c-Met and Pim-1 inhibitory activity. Based on the promising antiproliferative activities demonstrated by the synthesized benzylidene derivatives, future work will involve synthesizing new derivatives by incorporating heteroaryl aldehydes such as pyridine, pyrimidine, pyrazole, and imidazole. Additionally, various aryl groups with electron-withdrawing and electron-donating properties will be introduced to further explore and test their biological activities.

Data availability

The data supporting this article have been included as part of the ESI.†

Conflicts of interest

The authors have no conflicts of interest. This manuscript's content and writing are the sole responsibility of its authors.

Acknowledgements

The authors are grateful to the National Institute of Health, for their support of antiproliferative screening.

References

1 A. K. Kwakye, S. Kampo, J. Lv, M. N. Ramzan, S. A. Richard, A. A. Falagán, J. Agudogo, E. Atito-Narh, Q. Yan and Q. P. Wen, *BMC Res. Notes*, 2020, **13**, 386.
2 E. Y. Ahmed, O. M. Abdelhafez, D. Zaafar, A. M. Serry, Y. H. Ahmed, R. F. A. El-Telbany, Z. Y. Abd Elmageed and H. I. Ali, *Arch. Pharm.*, 2022, **355**, 2100327.
3 R. Wang, J. Wang, T. Dong, J. Shen, X. Gao and J. Zhou, *Oncol. Lett.*, 2019, **17**, 1217–1222.
4 X. Liu, W. Yao, R. C. Newton and P. A. Scherle, *Expert Opin. Investig. Drugs*, 2008, **17**, 997–1011.
5 C. Schmidt, F. Bladt, S. Goedecke, V. Brlnkmann, W. Zschiesche, M. Sharpet, E. Gherardlt and C. Birchmelert, *Nature*, 1995, **373**, 699–702.

6 E. M. Ahmed, N. A. Khalil, A. T. Taher, R. H. Refaey and Y. M. Nissan, *Bioorg. Chem.*, 2019, **92**, 103272.
7 Y. Tursynbay, J. Zhang, Z. Li, T. Tokay, Z. Zhumadilov, D. Wu and Y. Xie, *Biomed. Rep.*, 2016, **4**, 140–146.
8 C. O. ning Leung, C. C. lui Wong, D. N. yin Fan, A. K. lun Kai, E. K. kwan Tung, I. M. jing Xu, I. O. lin Ng and R. C. lam Lo, *Oncotarget*, 2015, **6**, 10880–10892.
9 N. A. Keane, M. Reidy, A. Natoni, M. S. Raab and M. O'Dwyer, *Blood Cancer J.*, 2015, **5**, e325.
10 R. A. Darby, A. Unsworth, S. Knapp, I. D. Kerr and R. Callaghan, *Cancer Chemother. Pharmacol.*, 2015, **76**, 853–864.
11 B. Oyallon, M. Brachet-Botineau, C. Logé, T. Robert, S. Bach, S. Ibrahim, W. Raoul, C. Croix, P. Berthelot, J. Guillon, N. Pinaud, F. Gouilleux, M.-C. Viaud-Massuard and C. Denevault-Sabourin, *Molecules*, 2021, **26**, 867.
12 D. Reddy, R. Kumavath, P. Ghosh and D. Barh, *Biomolecules*, 2019, **9**, 792.
13 R. L. B. Costa, H. S. Han and W. J. Gradishar, *Breast Cancer Res. Treat.*, 2018, **169**, 397–406.
14 F. André, E. Ciruelos, G. Rubovszky, M. Campone, S. Loibl, H. S. Rugo, H. Iwata, P. Conte, I. A. Mayer, B. Kaufman, T. Yamashita, Y.-S. Lu, K. Inoue, M. Takahashi, Z. Pápai, A.-S. Longin, D. Mills, C. Wilke, S. Hirawat and D. Juric, *N. Engl. J. Med.*, 2019, **380**, 1929–1940.
15 N. C. Turner, E. Alarcón, A. C. Armstrong, M. Philco, Y. A. López Chuken, M. P. Sablin, K. Tamura, A. Gómez Villanueva, J. A. Pérez-Fidalgo, S. Y. A. Cheung, C. Corcoran, M. Cullberg, B. R. Davies, E. C. De Bruin, A. Foxley, J. P. O. Lindemann, R. Maudsley, M. Moschetta, E. Outhwaite, M. Pass, P. Rugman, G. Schiavon and M. Oliveira, *Ann. Oncol.*, 2019, **30**, 774–780.
16 R. W. Carling, A. Madin, A. Guiblin, M. G. N. Russell, K. W. Moore, A. Mitchinson, B. Sohal, A. Pike, S. M. Cook, I. C. Ragan, R. M. McKernan, K. Quirk, P. Ferris, G. Marshall, S. A. Thompson, K. A. Wafford, G. R. Dawson, J. R. Atack, T. Harrison, J. L. Castro and L. J. Street, *J. Med. Chem.*, 2005, **48**, 7089–7092.
17 R. W. Carling, K. W. Moore, L. J. Street, D. Wild, C. Isted, P. D. Leeson, S. Thomas, D. O'Connor, R. M. McKernan, K. Quirk, S. M. Cook, J. R. Atack, K. A. Wafford, S. A. Thompson, G. R. Dawson, P. Ferris and J. L. Castro, *J. Med. Chem.*, 2004, **47**, 1807–1822.
18 L. P. Guan, X. Sui, X. Q. Deng, Y. C. Quan and Z. S. Quan, *Eur. J. Med. Chem.*, 2010, **45**, 1746–1752.
19 J. S. Ruso, N. Rajendiran, C. Srinivas, K. N. Murthy and K. Soumya, *J. Korean Chem. Soc.*, 2014, **58**, 377–380.
20 M. Islam and A. A. Siddiqui, *Acta Pol. Pharm. – Drug Res.*, 2010, **67**, 555–562.
21 A. E. Rashad, A. H. Shamroukh, M. A. Ali and F. M. Abdel-Motti, *Heteroat. Chem.*, 2007, **18**, 274–282.
22 A. H. Shamroukh and M. A. Ali, *Arch. Pharm.*, 2008, **341**, 223–230.
23 P. Galatsis, J. L. Henderson, B. L. Kormos, S. Han, R. G. Kurumbail, T. T. Wager, P. R. Verhoest, G. S. Noell, Y. Chen, E. Needle, Z. Berger, S. J. Steyn, C. Houle and W. D. Hirst, *Bioorg. Med. Chem. Lett.*, 2014, **24**, 4132–4140.
24 M. Franzini, X. M. Ye, M. Adler, D. L. Aubele, A. W. Garofalo, S. Gauby, E. Goldbach, G. D. Probst, K. P. Quinn, P. Santiago, H. L. Sham, D. Tam, A. Truong and Z. Ren, *Bioorg. Med. Chem. Lett.*, 2013, **23**, 1967–1973.
25 A. P. Skoumbourdis, C. A. LeClair, E. Stefan, A. G. Turjanski, W. Maguire, S. A. Titus, R. Huang, D. S. Auld, J. Inglese, C. P. Austin, S. W. Michnick, M. Xia and C. J. Thomas, *Bioorg. Med. Chem. Lett.*, 2009, **19**, 3686–3692.
26 J. K. Brenke, G. M. Popowicz, K. Schorpp, I. Rothenaigner, M. Roesner, I. Meininger, C. Kalinski, L. Ringelstetter, O. R'kyek, M. Vincendeau, O. Plettenburg, M. Sattler, D. Krappmann, K. Hadian and G. Jürjens, *J. Biol. Chem.*, 2018, **293**, 13191–13203.
27 F. Jin, Y. Lin, W. Yuan, S. Wu, M. Yang, S. Ding, J. Liu and Y. Chen, *Eur. J. Med. Chem.*, 2024, **272**, 116477.
28 B. K. Albrecht, J. C. Harmange, D. Bauer, L. Berry, C. Bode, A. A. Boezio, A. Chen, D. Choquette, I. Dussault, C. Fridrich, S. Hirai, D. Hoffman, J. F. Larrow, P. Kaplan-Lefko, J. Lin, J. Lohman, A. M. Long, J. Moriguchi, A. O'Connor, M. H. Potashman, M. Reese, K. Rex, A. Siegmund, K. Shah, R. Shimanovich, S. K. Springer, Y. Teffera, Y. Yang, Y. Zhang and S. F. Bellon, *J. Med. Chem.*, 2008, **51**, 2879–2882.
29 R. Grey, A. C. Pierce, G. W. Bemis, M. D. Jacobs, C. S. Moody, R. Jajoo, N. Mohal and J. Green, *Bioorg. Med. Chem. Lett.*, 2009, **19**, 3019–3022.
30 S. E. Seif, Z. Mahmoud, W. W. Wardakhan, A. M. Abdou and R. A. Hassan, *Drug Dev. Res.*, 2023, **84**, 839–860.
31 M. T. M. Sayed, P. A. Halim, A. K. El-Ansary and R. A. Hassan, *Drug Dev. Res.*, 2023, **84**, 1299–1319.
32 W. E. Elgammal, S. S. Shaban, E. M. Eliwa, A. H. Halawa, S. M. A. El-gilil, R. A. Hassan, A. M. Abdou, G. A. M. Elhagali and M. Abdel Reheim, *Future Med. Chem.*, 2024, 1–19.
33 M. M. Zeid, O. M. El-Badry, S. Elmeligie and R. A. Hassan, *Chem. Biodivers.*, 2024, **21**, e202400077.
34 S. H. Emam, R. A. Hassan, E. O. Osman, M. I. A. Hamed, A. M. Abdou, M. M. Kandil, E. M. Elbaz and D. S. Mikhail, *Drug Dev. Res.*, 2023, **84**, 475–499.
35 E. O. Osman, S. H. Emam, A. Sonousi, M. M. Kandil, A. M. Abdou and R. A. Hassan, *Drug Dev. Res.*, 2023, **84**, 888–906.
36 A. Sonousi, R. A. Hassan, E. O. Osman, A. M. Abdou and S. H. Emam, *J. Enzyme Inhib. Med. Chem.*, 2022, **37**, 2644–2659.
37 S. Y. Ewieda, R. A. Hassan, E. M. Ahmed, A. M. Abdou and M. S. A. Hassan, *Bioorg. Chem.*, 2024, **150**, 107623–107635.
38 Z. Arghiani, S. M. Seyedi, M. Bakavoli and H. Eshghi, *J. Heterocycl. Chem.*, 2015, **52**, 1099–1107.
39 W. R. Carling, J. L. C. Pineiro, I. J. Collins, A. R. Guiblin, T. Harrison, A. Madin, K. W. Moore, M. G. Russell, G. Scott and L. J. Street, *US Pat.*, 6828322, 2004.
40 R. Aggarwal, Mamta, G. Sumran and M. C. Torralba, *J. Mol. Struct.*, 2019, **1185**, 379–391.
41 P. Skehan, R. Storeng, D. Scudiero, A. Monks, J. McMahon, D. Vistica, J. T. Warren, H. Bokesch, S. Kenney and M. R. Boyd, *J. Natl. Cancer Inst.*, 1990, **82**, 1107–1112.
42 R. H. Shoemaker, *Nat. Rev. Cancer*, 2006, **6**, 813–823.

43 M. R. Boyd and K. D. Paull, *Drug Dev. Res.*, 1995, **34**, 91–109.
44 M. C. Alley, D. A. Scudiere, A. Monks, M. L. Hursey, M. J. Czerwinski, D. L. Fine, B. J. Abbott, J. G. Mayo, R. H. Shoemaker and M. R. Boyd, *Cancer Res.*, 1988, **48**, 589–601.
45 M. R. Grever, S. A. Schepartz and B. A. Chabner, *Semin. Oncol.*, 1992, **19**, 622–638.
46 T. Mosmann, *J. Immunol. Methods*, 1983, **65**, 55–63.
47 L. Gong, Y. Tang, R. An, M. Lin, L. Chen and J. Du, *Cell Death Dis.*, 2017, **8**, e3080.
48 M. F. Tolba, A. Esmat, A. M. Al-Abd, S. S. Azab, A. E. Khalifa, H. A. Mosli, S. Z. Abdel-Rahman and A. B. Abdel-Naim, *IUBMB Life*, 2013, **65**, 716–729.
49 I. Vermes, C. Haanen, H. Steffens-Nakken and C. Reutellingsperger, *J. Immunol. Methods*, 1995, **184**, 39–51.
50 T. H. Ibrahim, Y. M. Loksha, H. A. Elshihawy, D. M. Khodeer and M. M. Said, *Arch. Pharm.*, 2017, **350**, e1700093.
51 A. Daina, O. Michielin and V. Zoete, *Sci. Rep.*, 2017, **7**, 42717.
52 A. Daina and V. Zoete, *ChemMedChem Commun.*, 2016, **11**, 1117–1121.